Vietnamese-German University

COPYRIGHT WARNING

RUHR-UNIVERSITÄT BOCHUM

MechEng
Mechanical Engineering

Vietnamese-German University

RUHR-UNIVERSITY BOCHUM
VIETNAMESE-GERMAN UNIVERSITY

BACHELOR THESIS

in

MECHANICAL ENGINEERING

Flow of kaolinite suspension in a sudden expansion channel

Author:
Nguyen Luong Khang

RUB Student ID: 19218821
VGU Student ID: 14574

Supervisor:
Assoc. Prof.,
Dr. Thinh Xuan Ho

Mechanical Engineering

December 02, 2023

Declaration of Authorship

I, Khang Nguyen Luong, declare that this thesis titled "Flow of kaolinite suspension in a sudden expansion channel" and the work presented in it are my own. I confirm that:

- The entirety of this work was completed while applying to this university for a bachelor's degree.
- It has been stated whether any portion of this thesis has ever been submitted for credit toward a degree or other qualification at this university or another.
- Whenever I have referenced someone else's published work, I always provide due credit.
- I have always cited my sources when I have used their words in my writing. This thesis is completely my own work, with the exception of such quotes.
- I have given credit to all sources of support.
- If the thesis is based on work I did in collaboration with others, I have explicitly stated what I contributed and what others did.

Signed:

_____

Date:

_____

Abstract

Kaolinite, a clay mineral of significance in various industrial contexts, introduces unique challenges to fluid dynamics due to its particulate nature. The investigation centers on unraveling the intricate interplay between the rheological characteristics of kaolinite suspension and the geometric attributes of a sudden expansion channel across a Reynolds number range of 20 to 100. The outcomes of this research contribute to an enhanced comprehension of kaolinite suspension dynamics, offering potential optimizations for industrial processes.

In this thesis, a numerical approach is utilized to explore the behavior of a water–kaolinite suspension characterized by varying kaolinite concentrations, specifically 15wt%, 20wt%, and 28.5wt%. The suspension is conceptualized as a Bingham fluid, drawing upon rheological data obtained from existing literature. The chosen Bingham fluid model provides a well-founded basis for simulating the viscoplastic behavior of the suspension, paving the way for a comprehensive understanding of its rheological response across a spectrum of concentrations.

The meshing process is carefully undertaken to ensure accuracy and computational efficiency. The simulation tool employed for this investigation is ANSYS Fluent, a widely recognized and extensively utilized computational fluid dynamics (CFD) software. The chosen simulation domain is characterized by a sudden expansion with a geometric ratio of 3, a pivotal aspect influencing the overall flow dynamics.

Following a sudden expansion, symmetric recirculations are observed in Kao-fluids at corners, resembling the behavior of n = 1 power-law fluids at low Reynolds numbers. The examination of the characteristic length for different Kao-fluids and the analysis of velocity profiles for each fluid are conducted. Additionally, a comparative analysis between simulation and theoretical results is performed for the Darcy friction factor of the working fluids.

Acknowledgements

I would like to sincerely thank Dr. Thinh Xuan Ho, a lecturer at Vietnamese-German University (VGU)'s Faculty of Engineering, for agreeing to supervise my thesis. I completed this thesis because of his diligent guidance.

Next, I would like to express my gratitude to the professors and lecturers in the Mechanical Engineering program at the Vietnamese-German University, Otto von Guericke University in Magdeburg, and Ruhr University Bochum for their expertise that helped me to achieve my thesis.

Lastly, I would appreciate my friends and family who assisted me with the process of completing my thesis.

Contents

Dedicated to my parents, Thuong Nguyen Dinh and Nhan Pham Thi Thanh, and my two sisters.

Chapter 1

Introduction

1.1 Non-Newtonian fluid

1.1.1 Definition

A fluid is a substance that changes shape when subjected to shear stress or an external force. Liquid and gas can be categorized as fluid, which are found vastly in the nature and technical applications such as: turbines and pumps, waterfall, air-conditioner, mechanical wings, etc.

$$\tau = \mu\left(\frac{du}{dy}\right) = \mu\dot{\gamma} \tag{1.1}$$

Viscosity, a measure of a fluid's resistance to deformation, is used in the study of different types of fluids to classify them. Newtonian fluids have constant viscosity because of the linear relationship between shear stress and shear rate, as described by Newton's Law of Viscosity above.

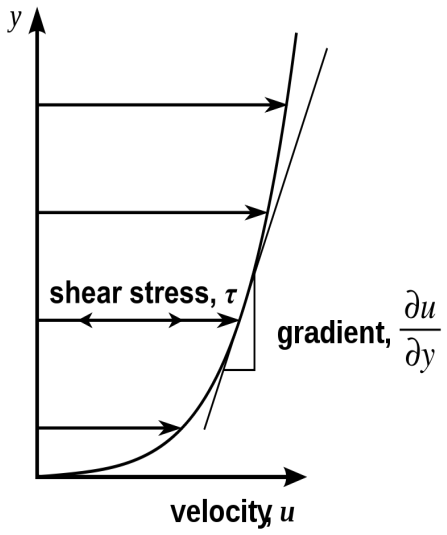

FIGURE 1.1: The relationship between shear stress and velocity gradient [1].

Non-Newtonian fluids adjust viscosity under shear stress, being either more liquid or more solid. These fluids have complicated rheological features include yield stress, viscoelasticity, and thixotropy. A viscoplastic fluid is one that flows only when the shear stress surpasses a value known as the yield stress.

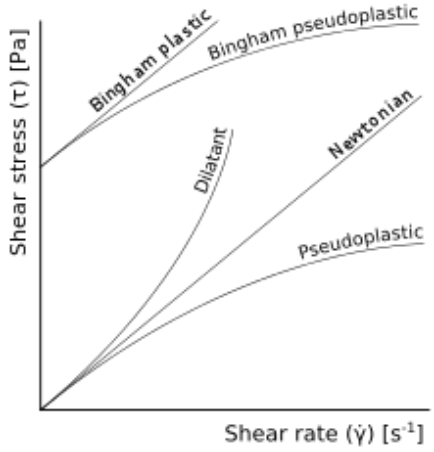

FIGURE 1.2: Classification of non-Newtonian fluids [2].

Below are three types of time-independent non-Newtonian fluid behavior:

Type	**Mathematical Model**
Shear-thinning or pseudoplastic fluids	Power-law model: $\tau = K\left(\frac{du}{dy}\right)^n$ $\eta = K\left\lvert\frac{du}{dy}\right\rvert^{n-1}$, with $n < 1$
Viscoplastic fluid behavior	Bingham plastic model: $\frac{\partial u}{\partial y} = \begin{cases} 0, & \text{if } \tau < \tau_0 \\ \frac{\tau - \tau_0}{\mu_\infty}, & \text{if } \tau \geq \tau_0 \end{cases}$
Shear-thickening or dilatant fluid behavior	Power-law model: $\tau = K\left(\frac{du}{dy}\right)^n$ $\eta = K\left\lvert\frac{du}{dy}\right\rvert^{n-1}$, with $n > 1$

TABLE 1.1: Mathematical Models for Different Fluid Behaviors [3]

This study focuses on the behaviour of non-Newtonian fluids through a sudden expansion: three Bingham fluids which are Kaolinite 15, 20 and 28.5.

1.1.2 Applications

We come into contact with non-Newtonian fluids more often than we imagine. Non-Newtonian fluids are present in a variety of goods.

Smart fluids

Smart fluids are fluids that change their properties (e.g. viscosity) under the effect of an electric field or a magnetic field. Two example for these fluids are the electrorheological fluid (ErF) and the magnetorheological fluid (MrF). In reaction to an electric field, the viscosity of an ErF can change incredibly fast. As a result, it is used in quick-response hydraulic valves. The magnetorheological damper is created using MrF. This damper enables for continuous modification of the shock absorber's damping characteristic by varying the magnetic field intensity. So it is used for stress absorption in prosthetic legs as well as vehicles such as cars and helicopters.

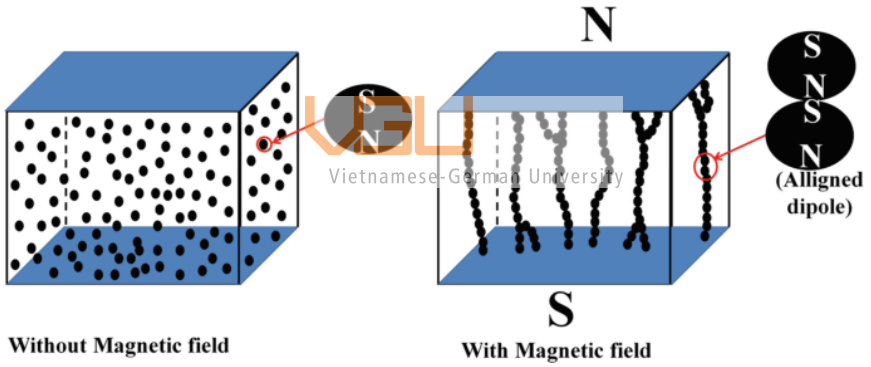

FIGURE 1.3: Smart fluid mechanism [4].

Artificial organs

The medical field advances via the study of non-Newtonian fluid. Human organs that are synthetic have been developed and mostly used in cases of organ failure, work exactly like their natural counterparts, the heart, kidneys, and livers. Artificial organs are used to replace the donor organs entirely in the event that transplantation is not feasible, or to bridge the transplantation gap. The avoidance of blood clotting is a crucial use for the construction of these artificial organs. This was made possible by studies on blood, a non-Newtonian fluid.

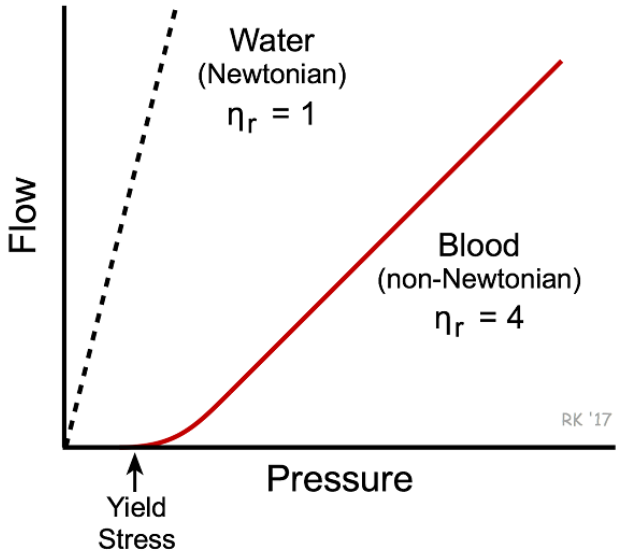

FIGURE 1.4: Viscosity of blood [5].

Food

Aside from these uses, non-Newtonian fluid behavior may be seen in foods such as low-fat mayonnaise, yogurt, jam, ketchup and so on. Alginate stabilized thixotropic gels are frequently used to stabilize emulsions and the consistency of foods like ice cream.

FIGURE 1.5: An example in food product [6].

1.2 Literature review

When a Newtonian fluid undergoes a sudden expansion at low to moderate Reynolds numbers, the resulting flow exhibits a pair of symmetric recirculating swirls along the downstream walls. The symmetry of these vortices transitions to asymmetry when the Reynolds number (Re) surpasses a critical value. In the case of planar geometry, the expansion ratio (ER) is denoted as the ratio of the height of the outlet channel (H) to the height of the input channel (h).

The phenomenon of flow bifurcation in channels featuring a sudden planar expansion has been a subject of numerous experimental investigations dating back to the early 1970s. Durst et al. [7] and Cherdron et al. [8] employed laser Doppler anemometry (LDA) to examine the impact of the aspect ratio of the tested geometry and to observe vortices at both salient corners. In a more recent study, Fearn et al. [9] explored a planar expansion with an expansion ratio (ER) of 3, revealing an identical flow bifurcation occurring at $Re = 40.5$. Drikakis [10] noted in his investigation that an increase in the expansion ratio leads to a reduction in the critical Reynolds number for the symmetry-breaking bifurcation, considering various ratios. All of these investigations were specifically focused on Newtonian fluids.

In practical situations, fluids coursing through pipes deviate from Newtonian behavior and present intricate rheological characteristics. Depending on the type of fluid, these may include shear-thinning or shear-thickening viscosity. Consequently, delving into the realm of non-Newtonian fluid flow in planar expansions becomes imperative. Commencing with fundamental rheological models is essential to comprehend the influence of diverse rheological properties on flow characteristics. Elevated Reynolds numbers have the potential to induce turbulent flow, particularly when the non-Newtonian solutions are not highly concentrated. Given the well-established significance of sudden expansion geometry in studying laminar flow instabilities at high Reynolds numbers, it has naturally captivated the interest of researchers in non-Newtonian fluid mechanics. Their focus centers on unraveling the intricate interplay between these bifurcations and fluid rheology, with a specific emphasis on viscoelasticity. Notably, the study of non-Newtonian blood flow in arterial stenoses and abdominal aneurysms is directly connected to the investigation of flow in expansions.

Multiple numerical investigations have utilized the power-law viscosity model to scrutinize the flow behavior of shear-thinning and shear-thickening fluids in planar sudden expansions. This model, characterized by its simplicity, proves particularly effective for describing the traits of shear-thinning, shear-thickening, and Newtonian fluids. By adjusting the power-law index n, the model adeptly captures the distinctive characteristics of these fluid types within a purely viscous solution.

Mishra and Jayaraman [11] studied the characteristics of steady asymmetric flow patterns in shear-thinning fluids within planar sudden expansions with a high expansion ratio ($ER = 16$). In a separate investigation, Manica and De Bortoli [12] employed numerical methods to analyze the flow of power-law fluids in a planar sudden expansion with $ER = 3$ for various power-law indices (n: 0.5, 1, and 1.5). Their study explored vortex properties for these n values within a Reynolds number range of $30 \leq Re \leq 125$. The results indicated that shear-thickening fluids exhibited the lowest critical Reynolds number, and the flow bifurcation for shear-thinning fluids occurred at a critical Reynolds number higher than that for Newtonian fluids. Furthermore, Neofytou [13] investigated the influence of Reynolds number on flow patterns and the transition from symmetric to asymmetric flow in power-law fluids, considering power-law indices in the range $0.3 \leq n \leq 3$, within a planar sudden expansion with $ER = 2$.

Numerous researchers have endeavored to employ both commercial and open-source algorithms for numerical simulations of power-law fluid flow in a planar sudden expansion with $ER = 3$. It has been observed that achieving convergence in the solutions can be a substantial challenge, especially when dealing with pronounced non-Newtonian behavior, characterized by either large or small values of n in the power-law model. Poole and Ridley [14] utilized Fluent software, reporting an inability to attain a converged solution for $n < 0.4$. Similarly, Ternik et al. [15] asserted that no converged solutions were obtained for $n < 0.6$ when utilizing the OpenFOAM software.

1.3 Objectives

The thesis is going on studying about the flow of three Kaolinite fluids through a sudden expansion by using ANSYS Fluent as the simulation software:

- Chapter 2 describes governing equations, fluid properties, and numerical method used in this study.
- Chapter 3 details the domain, the using mesh and the simulation settings.
- Chapter 4, the simulation results are discussed.
- Chapter 5 presents final remarks on the analysis.

Chapter 2

Background theory

2.1 Problem description

The study case is illustrated by the figure 2.1. A small channel of width h expands to the bigger one of width H, with the ratio $ER = H/h = 3:1$. The origin of the y co-ordinate is lied at the center of two channels. The small channel's length is $L_C = 50h$ and the large one is $L_E = 150h$.

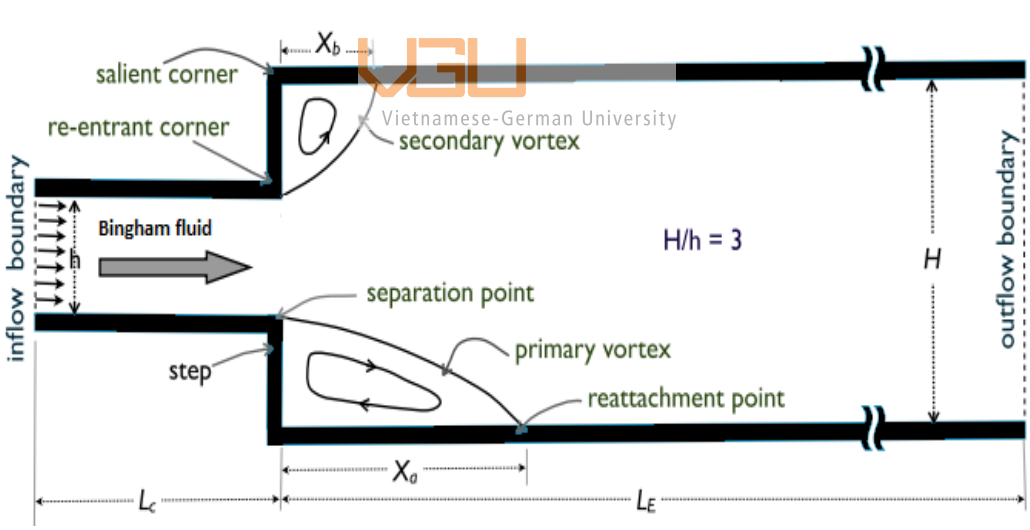

FIGURE 2.1: Two-dimensional 3:1 sudden planar expansion diagram. Adopted from Dhinakaran et al. [16]

The inlet is far from the expansion location to ensure that the flow to become fully developed before the interest incident occurs. It is the same for the outlet to be located far from expansion plane.

2.2 Governing equations

The continuity equation governs the 2D laminar, steady and incompressible flow

$$\frac{\partial u}{\partial x} + \frac{\partial v}{\partial y} = 0 \tag{2.1}$$

with the momentum equations:

$$\rho\left(\frac{\partial u}{\partial t} + u\frac{\partial u}{\partial x} + v\frac{\partial u}{\partial y}\right) = -\frac{\partial p}{\partial x} + \left(\frac{\partial \tau_{xx}}{\partial x} + \frac{\partial \tau_{xy}}{\partial y}\right) \tag{2.2}$$

$$\rho\left(\frac{\partial v}{\partial t} + u\frac{\partial v}{\partial x} + v\frac{\partial v}{\partial y}\right) = -\frac{\partial p}{\partial y} + \left(\frac{\partial \tau_{xy}}{\partial x} + \frac{\partial \tau_{yy}}{\partial y}\right) \tag{2.3}$$

respectively, u and v indicate the velocity factors in the x and y directions; p is the pressure and ρ is the density.

The Bingham fluid model behaves like a Newtonian fluid when it flows, the shear rate is proportional to the applied shear stress. Otherwise, if the applied shear stress does not exceed the yield stress at a part, it will stay still.

$$\frac{\partial u}{\partial y} = \begin{cases} 0, & \text{if } \tau < \tau_0 \\ \frac{\tau - \tau_0}{\mu_\infty}, & \text{if } \tau \geq \tau_0 \end{cases} \tag{2.4}$$

These fluids in this work are Bingham fluid models have the same power-law index, $n = 1$ and the same critical shear rate 0.01.

Fluid	Density	Viscosity, K	Yield stress
Kao 15	1101.694915	0.001182007	0.08
Kao 20	1140.350877	0.001265640	0.4
Kao 28.5	1212.686567	0.001450325	2

TABLE 2.1: Properties of three Kaolinite 15, 20, 28.5

The pressure drop (ΔP) can be accurately determined using the Darcy–Weisbach equation[17]:

$$\frac{\Delta p}{L} = f_{\mathrm{D}} \cdot \frac{\rho}{2} \cdot \frac{\overline{v}^2}{D_H} \tag{2.5}$$

Where:

- $\frac{\Delta p}{L}$ is the pressure loss per unit length (SI units: Pa/m).

- f_{D} is the Darcy friction factor.
- ρ is the density of the fluid (SI units: kg/m³).
- D_H is the hydraulic diameter of the pipe (for a circular section, $D_H = 2h$ for the small section and $D_H = 2H$ for the large section; otherwise, $D_H = \frac{4A}{P}$ for a pipe of cross-sectional area A and perimeter P) (SI units: m).
- $\overline{v}$ is the mean flow velocity, experimentally measured as the volumetric flow rate Q per unit cross-sectional wetted area (SI units: m/s).

The friction loss for Bingham plastics in fully developed laminar pipe flow is described by the Buckingham–Reiner equation[18], expressed in a dimensionless form as follows:

$$f_{\mathrm{L}} = \frac{64}{\mathrm{Re}} \left[1 + \frac{\mathrm{He}}{6\mathrm{Re}} - \frac{64}{3} \left(\frac{\mathrm{He}^4}{f^3 \mathrm{Re}^7} \right) \right] \tag{2.6}$$

where:

- f_{L}: Laminar flow Darcy friction factor (SI units: dimensionless)
- Re: Reynolds number (SI units: dimensionless)
- He: Hedstrom number (SI units: dimensionless)

The Reynolds number and the Hedstrom number are respectively defined as:

$$\mathrm{Re} = \frac{\rho \overline{v} D}{\mu} \tag{2.7}$$

$$\mathrm{He} = \frac{\rho D^2 \tau_o}{\mu^2} \tag{2.8}$$

where:

- ρ: Mass density of the fluid (SI units: kg/m³)
- μ: Dynamic viscosity of the fluid (SI units: kg/m s)
- D: Diameter of circular pipe, here $D = h$ or $D = H$ (SI units: m)
- $\overline{v}$: Mean flow velocity (SI units: m/s)
- τ_o: Yield point (yield strength) of the fluid (SI units: Pa)

2.3 Simulation software

ANSYS Fluent is a computational fluid dynamics (CFD) software widely used for simulating fluid flow and heat transfer in engineering applications. The basis of it is the finite volume method, a numerical technique for resolving fluid flow-related partial differential equations. Renowned for its adaptability, ANSYS Fluent enables scientists and engineers to simulate a wide range of fluid dynamics situations, such as heat transfer, multiphase interactions, laminar and turbulent flows. Users of the program may study and visualize complicated fluid behavior in a variety of sectors, including manufacturing, aerospace, automotive, and energy. The software offers a full suite of tools for pre-processing, simulation, and post-processing.

A numerical method for resolving partial differential equations (PDEs), especially those that deal with fluid flow and heat transfer, is the Finite Volume Method (FVM). In simulations of computational fluid dynamics (CFD), it is often used. The following information pertains to the Finite Volume Method:

- Basic Principle: A continuous domain is discretized by FVM into a collection of discrete control volumes. These control volumes form the building blocks for the numerical solution of PDEs.

- Control Volumes: The domain is divided into control volumes, each enclosing a finite portion of the domain. Integral quantities (mass, momentum, energy) are conserved within each control volume.

- Conservation Laws: FVM is based on the conservation laws of mass, momentum, and energy. These laws are converted into algebraic equations for each control volume.

- Integral Form of PDEs: governing PDEs are converted from their differential form to an integral form over each control volume using the Gauss divergence theorem.

- Discretization: The integral equations are then discretized by approximating the spatial and temporal derivatives with suitable difference schemes. Common discretization techniques include central differencing for spatial terms and explicit or implicit schemes for time integration.

- Control Volume Balance: The conservation equations are applied to each control volume, leading to a system of algebraic equations. Fluxes

across the faces of the control volumes represent the interactions between neighboring volumes.

- Solver: The resulting system of algebraic equations is solved iteratively to obtain the solution at each discrete point in the domain. Iterative solvers, such as the SIMPLE (Semi-Implicit Method for Pressure-Linked Equations) algorithm, are often used in fluid flow simulations.
- Boundary Conditions: Boundary conditions are applied to the control volumes on the domain boundaries, specifying the behavior of the flow at those locations.
- Accuracy and Convergence: The accuracy of FVM depends on the grid resolution, with finer grids providing more accurate results. Convergence is achieved when the solution no longer changes significantly with each iteration.
- Applications: FVM is well-suited for a wide range of applications, including fluid flow, heat transfer, and combustion simulations. It is particularly popular in CFD due to its ability to handle complex geometries and conservation principles.

Chapter 3

Computational Implementation

Numerical simulations are worked with ANSYS Fluent 2023 R1, which is a Finite Volume-based software.

3.1 Computational domain and mesh

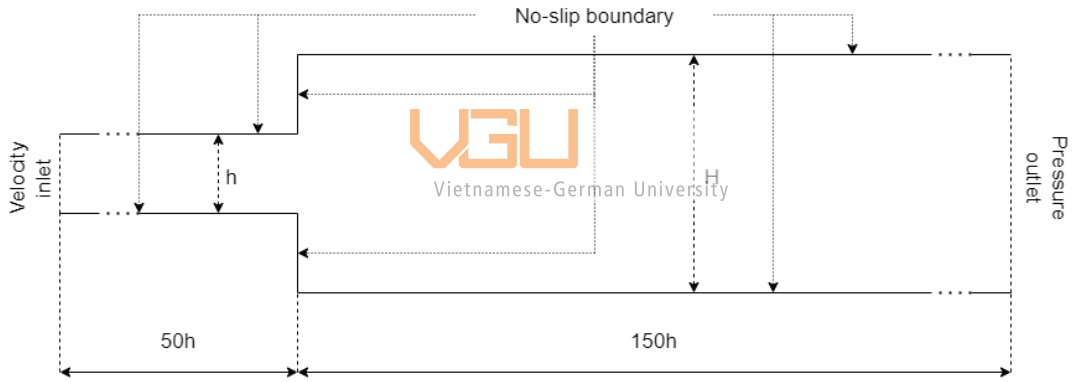

FIGURE 3.1: The domain of the flow

The domain for the working flow is defined as shown in Fig. 3.1. The inlet is configured with a velocity calculated from the Reynolds number and other fluid properties. The outlet is set as a pressure outlet, with the ambient pressure equal to 1 atmosphere (normal conditions). The smaller part of the tube is **50h** in length, while the larger part is **150h**. All walls are considered **no-slip** walls.

The structured mesh is used for the simulation. The mesh employed in this study plays a crucial role in accurately capturing the flow characteristics within the defined domain. A well-structured mesh is essential for achieving reliable and precise numerical simulations. In our analysis, a mesh comprising **124,450 cells** has been utilized. It provides sufficient accuracy to 1×10^{-7} with appropriate time-consuming for $Re \leq 100$. Fig. 3.2 gives an illustration of the used mesh.

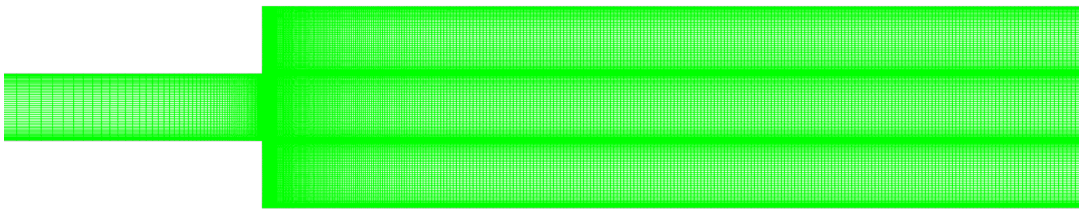

FIGURE 3.2: The utilized mesh

The mesh covers the entire computational domain, including both the smaller and larger sections of the tube. This thorough meshing approach allows for a detailed investigation of flow behaviors in various regions. The utilization of **no-slip** walls in the simulation ensures that the fluid interacts realistically with the boundaries, enhancing the accuracy of the results.

Additionally, the mesh is non-uniform, featuring higher resolution near the walls and the sudden expansion region. In contrast, lower resolution is applied in other regions. The intentional decision is to refine the mesh in areas where there are notable alterations in flow or boundary effects. This ensures a more accurate representation of how the fluid behaves in these crucial zones.

3.2 Solver setups

The mesh is drawn in millimeter for convenient purpose, but when it comes to the real case it must be scaled to the meter unit, as is shown in the Fig. 3.3

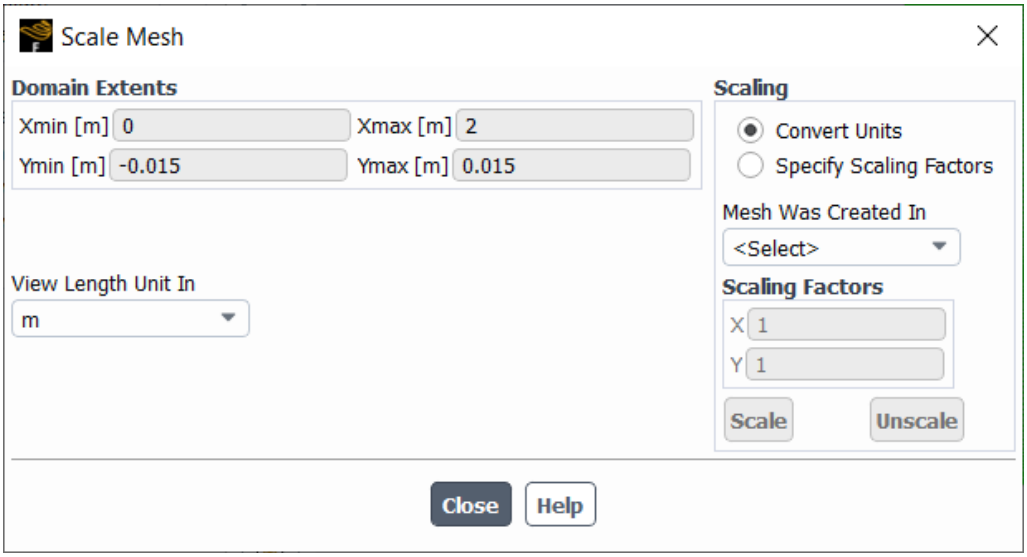

FIGURE 3.3: Scaling the mesh

The velocity inlet must be included in the reference value in the set up process of the Fluent application:

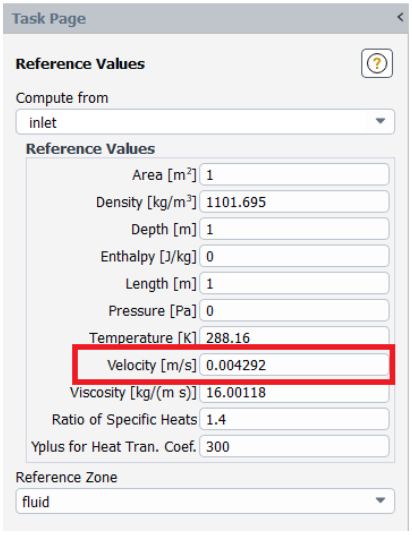

FIGURE 3.4: Setting up the velocity inlet

Then, the viscous model should be chosen as laminar

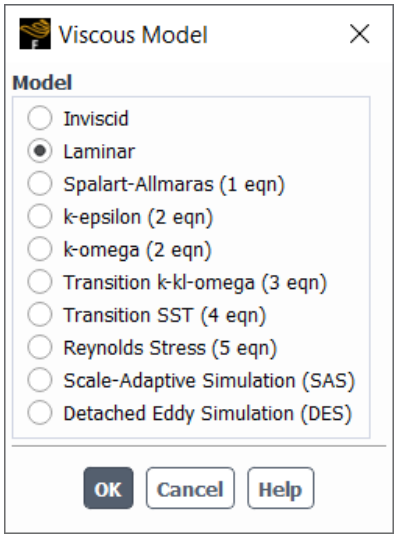

FIGURE 3.5: Choosing viscous model

For boundary conditions, all walls must be set to wall as stand for stationary wall. The inlet is velocity inlet and the outlet is pressure outlet.

The solution method that was used is SIMPLE. While alternative methods, such as Couple, have been explored, their significant time requirements make it impractical to execute the simulation on standard computational power.

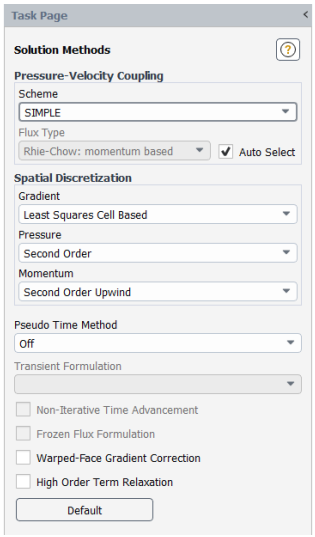

FIGURE 3.6: Selecting the method

The default residual values are set at 1×10^{-6}. However, to enhance the accuracy of the results, this study extends the range to 1×10^{-7}. Consequently, the residuals for continuity, x-velocity, and y-velocity need to be adjusted for each individual case during the simulation runs.

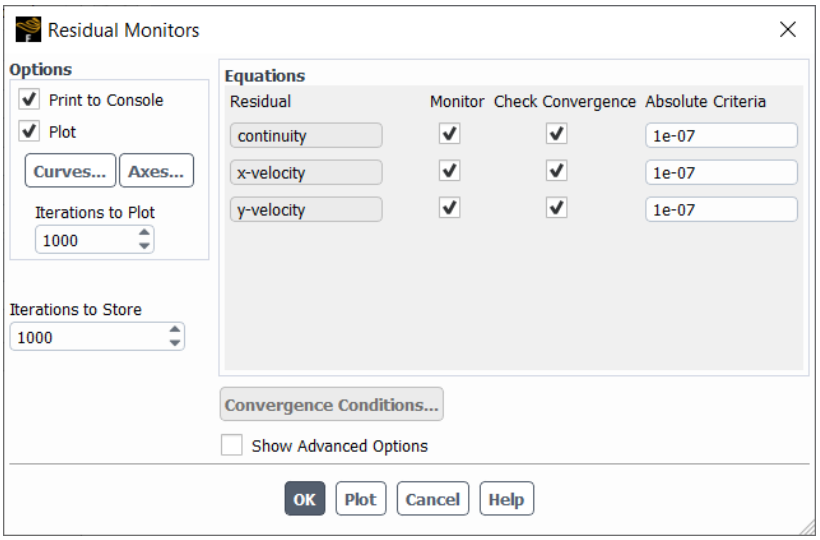

FIGURE 3.7: Adjusting the residual values

Regarding non-Newtonian fluids, running the solver directly is not feasible due to the absence of initial values for yield shear stress. Therefore, an initialization step becomes imperative. To make it close to the real case, the same density and viscosity (K) are employed for the first 100 steps. Subsequently, the viscosity is adjusted to Herschel-Bulkley, and the parameters for the power-law model are put in (Fig. 3.8).

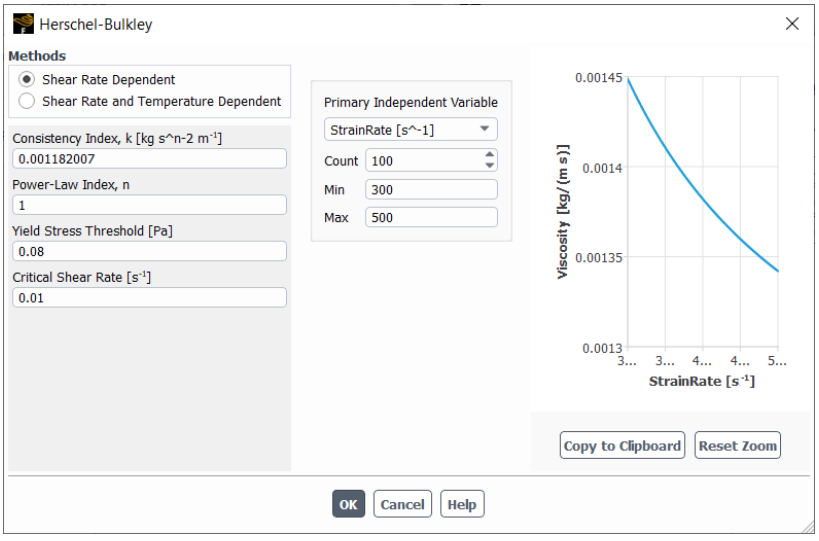

FIGURE 3.8: Bingham model material ($n = 1$)

Chapter 4

Result and discussion

4.1 Recirculation

4.1.1 Recirculation images

Doing the simulation of Kaolinite suspension of 15wt%, 20wt% and 28.5wt% in a sudden expansion of ratio 3 within the range of Reynolds number from 20 to 100 are carried out in this part. Various results for the streamline and velocity magnitudes are then discussed and analyzed.

As stated in Dhinakaran's work [16], the flow bifurcation into a sudden expansion for non-Newtonian fluids would result asymmetric recirculation at the bottom and top corner at large Reynolds number. However, for smaller Reynolds number, the shape of recirculations are symmetric with respect to the horizontal axis. This study is conducted at a low Reynolds number ($20 \leq Re \leq 100$) with the power-law index $n = 1$, so the symmetric shape is acquired.

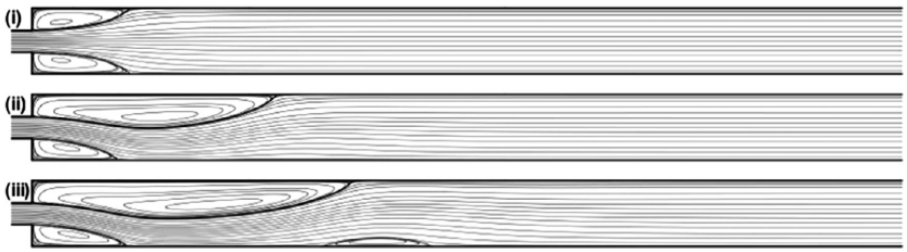

FIGURE 4.1: The streamline results in Dhinakaran et al. [16]

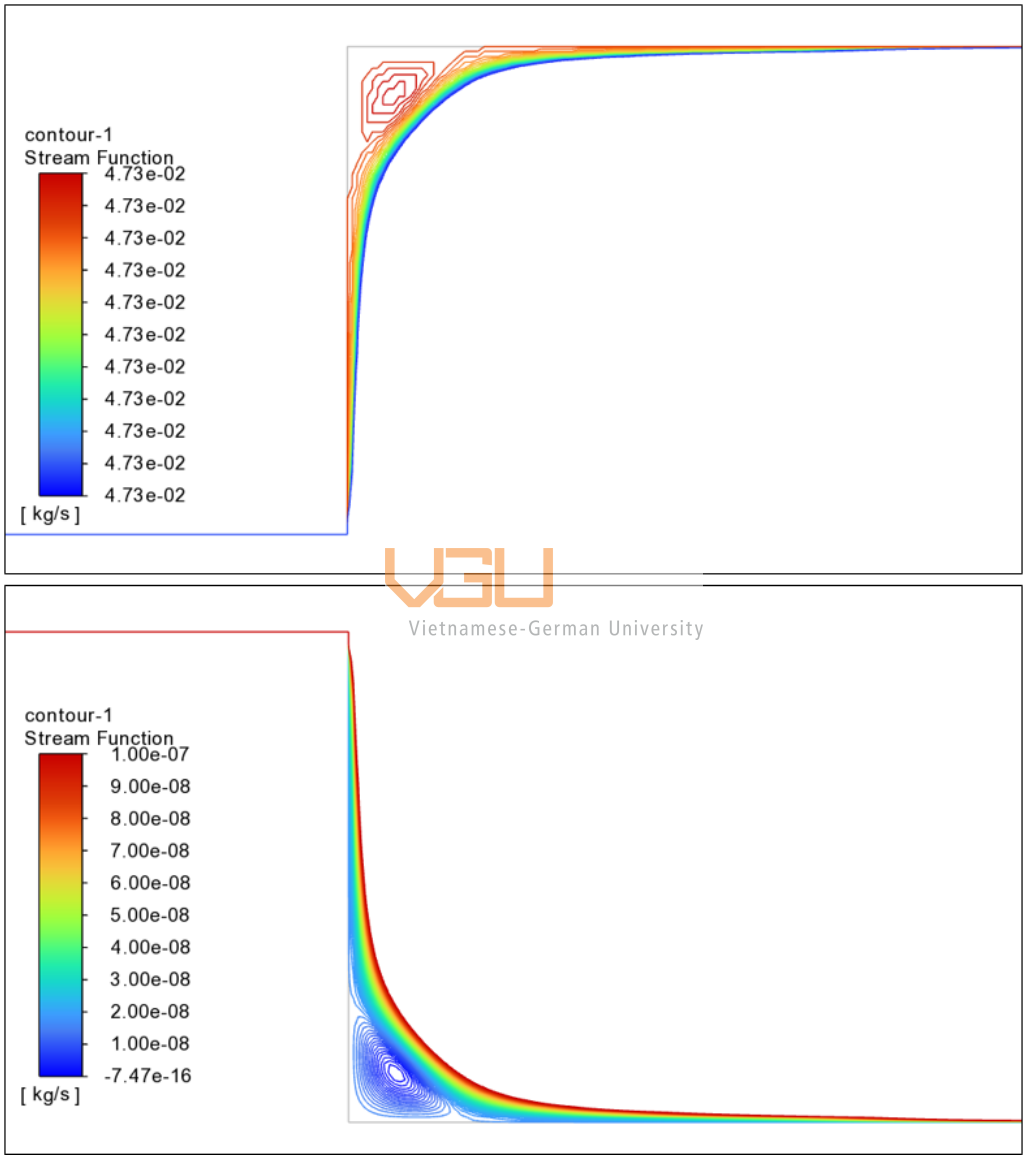

FIGURE 4.2: Recirculation of Kao 15wt% $Re = 40$

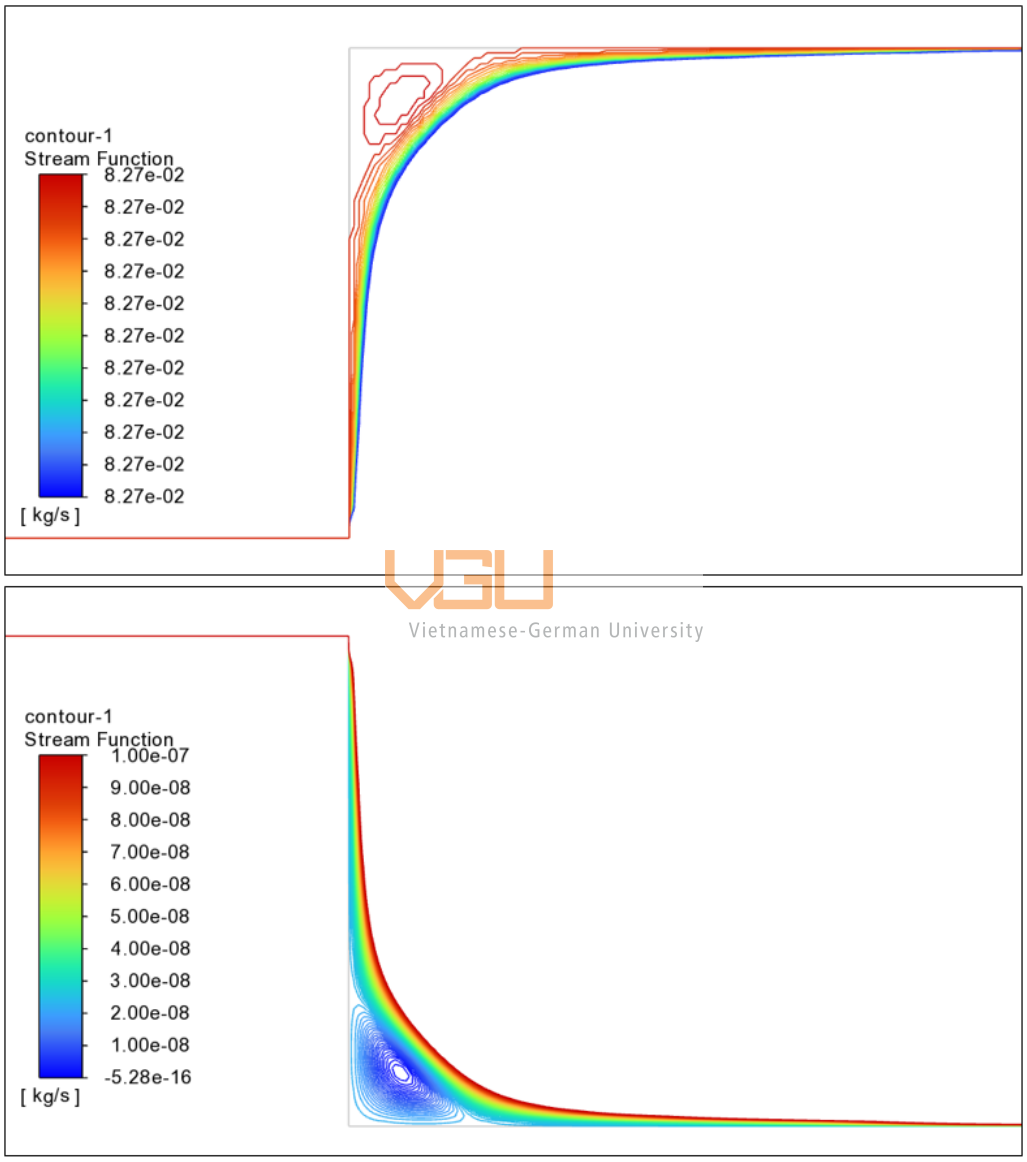

FIGURE 4.3: Recirculation of Kao 15wt% $Re = 70$

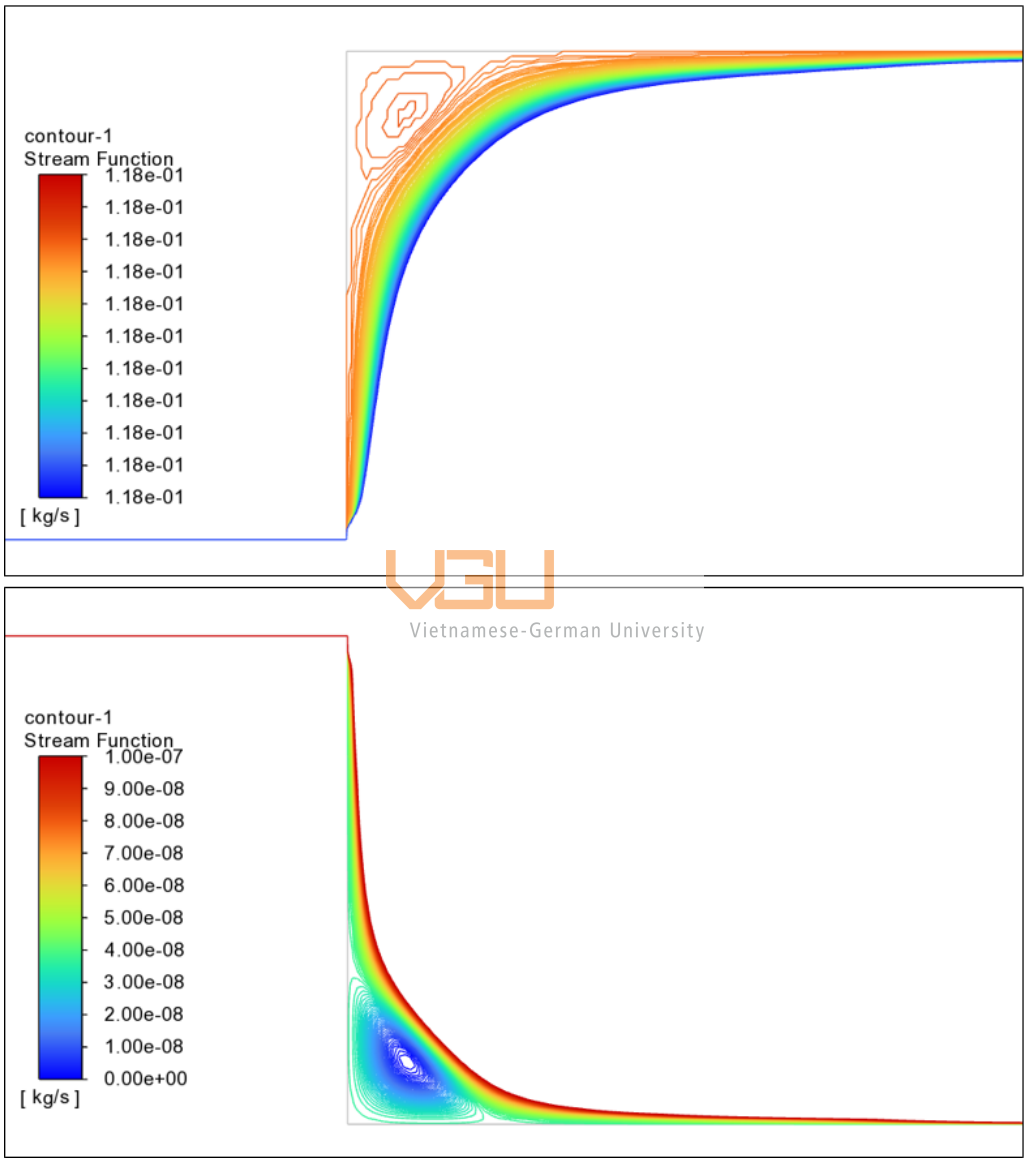

FIGURE 4.4: Recirculation of Kao 15wt% $Re = 100$

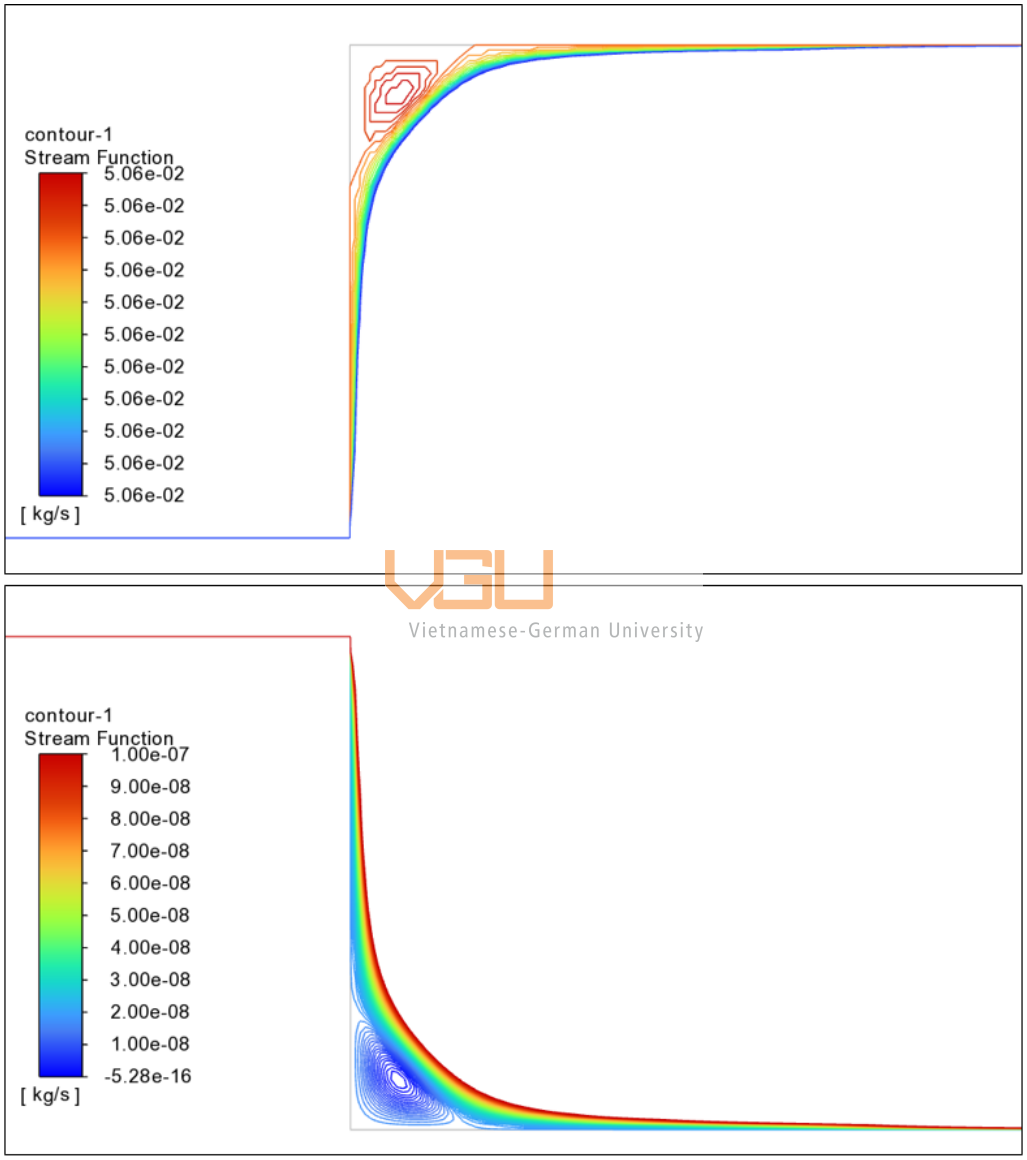

FIGURE 4.5: Recirculation of Kao 20wt% $Re = 40$

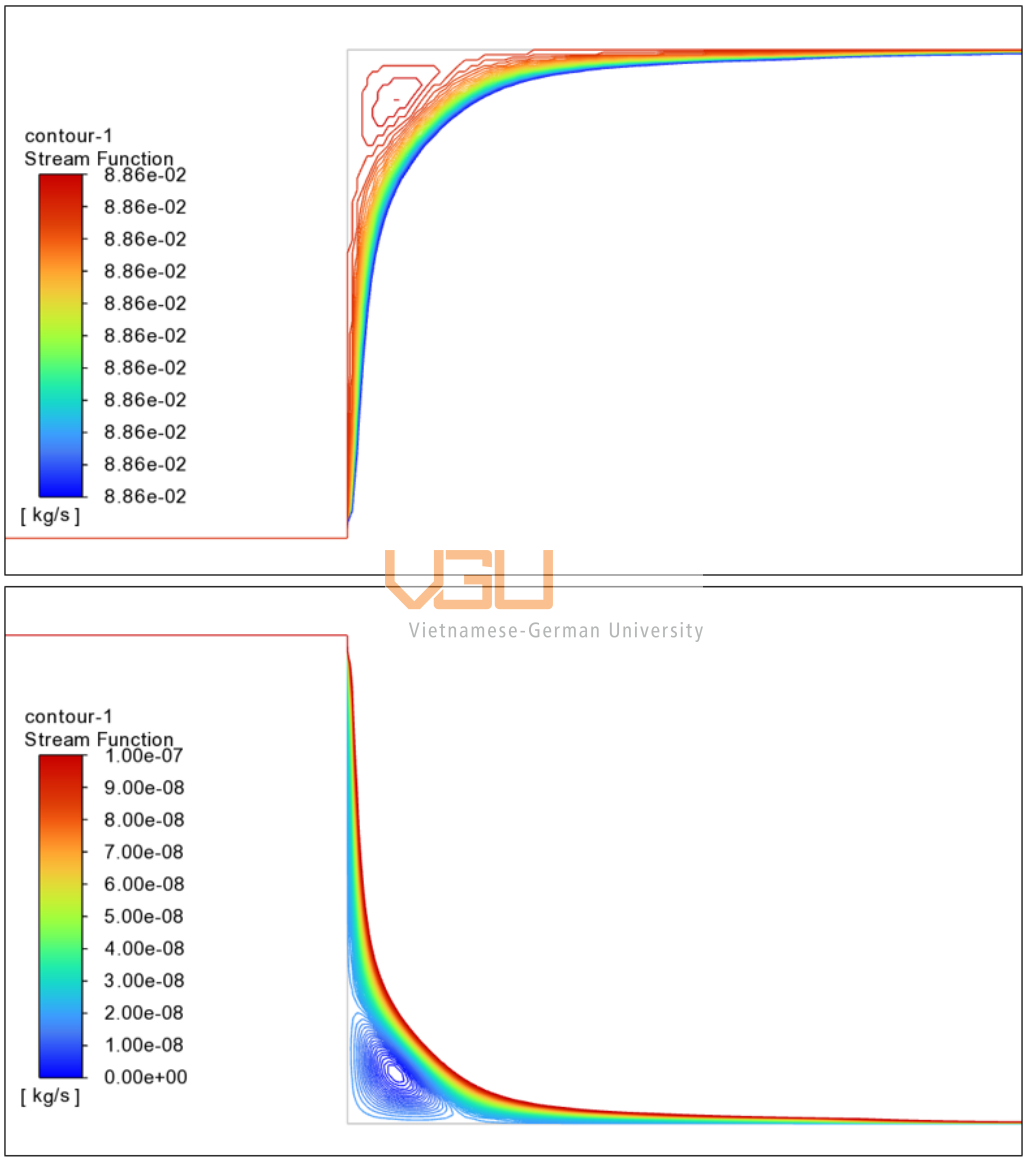

FIGURE 4.6: Recirculation of Kao 20wt% $Re = 70$

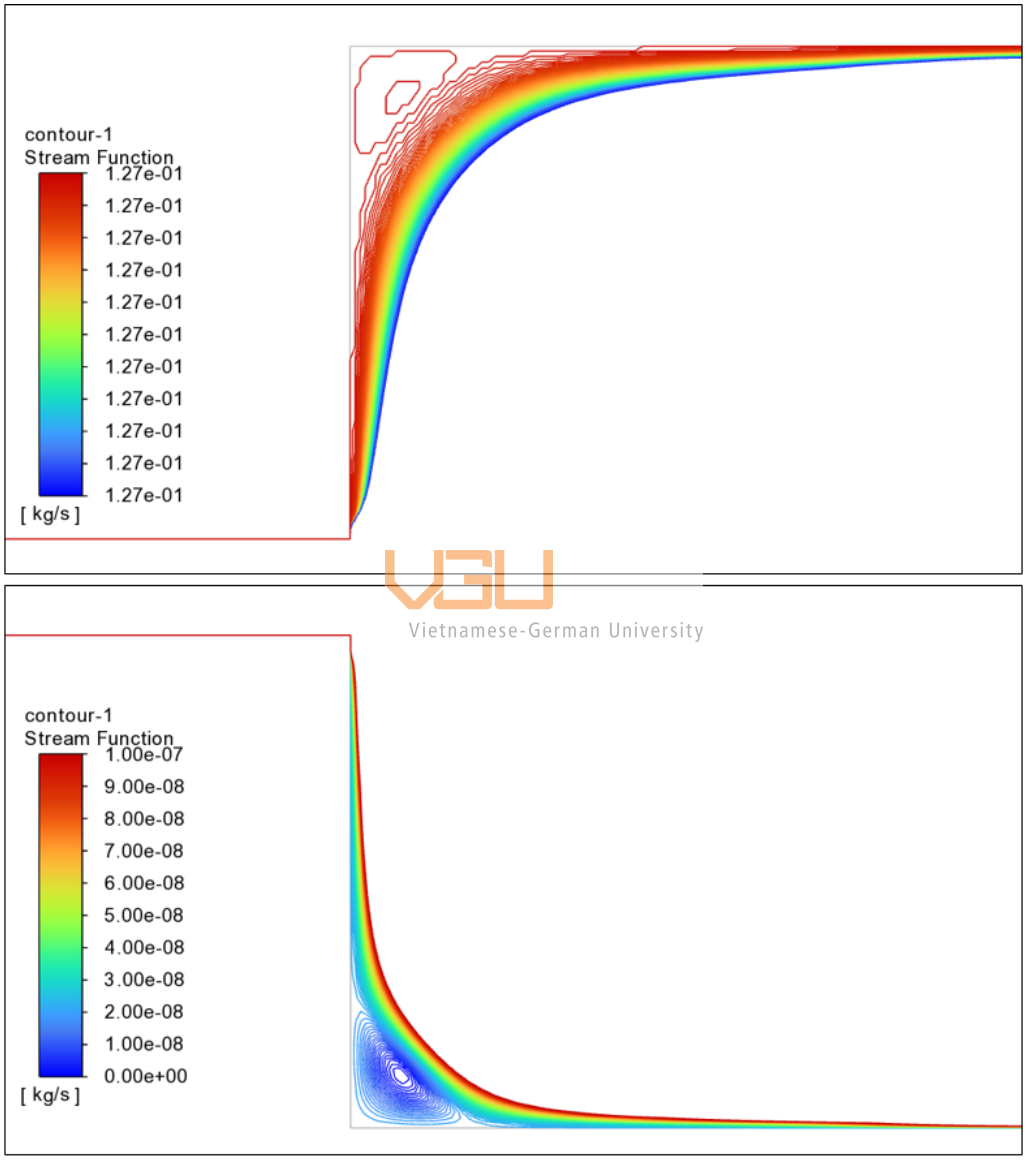

FIGURE 4.7: Recirculation of Kao 20wt% $Re = 100$

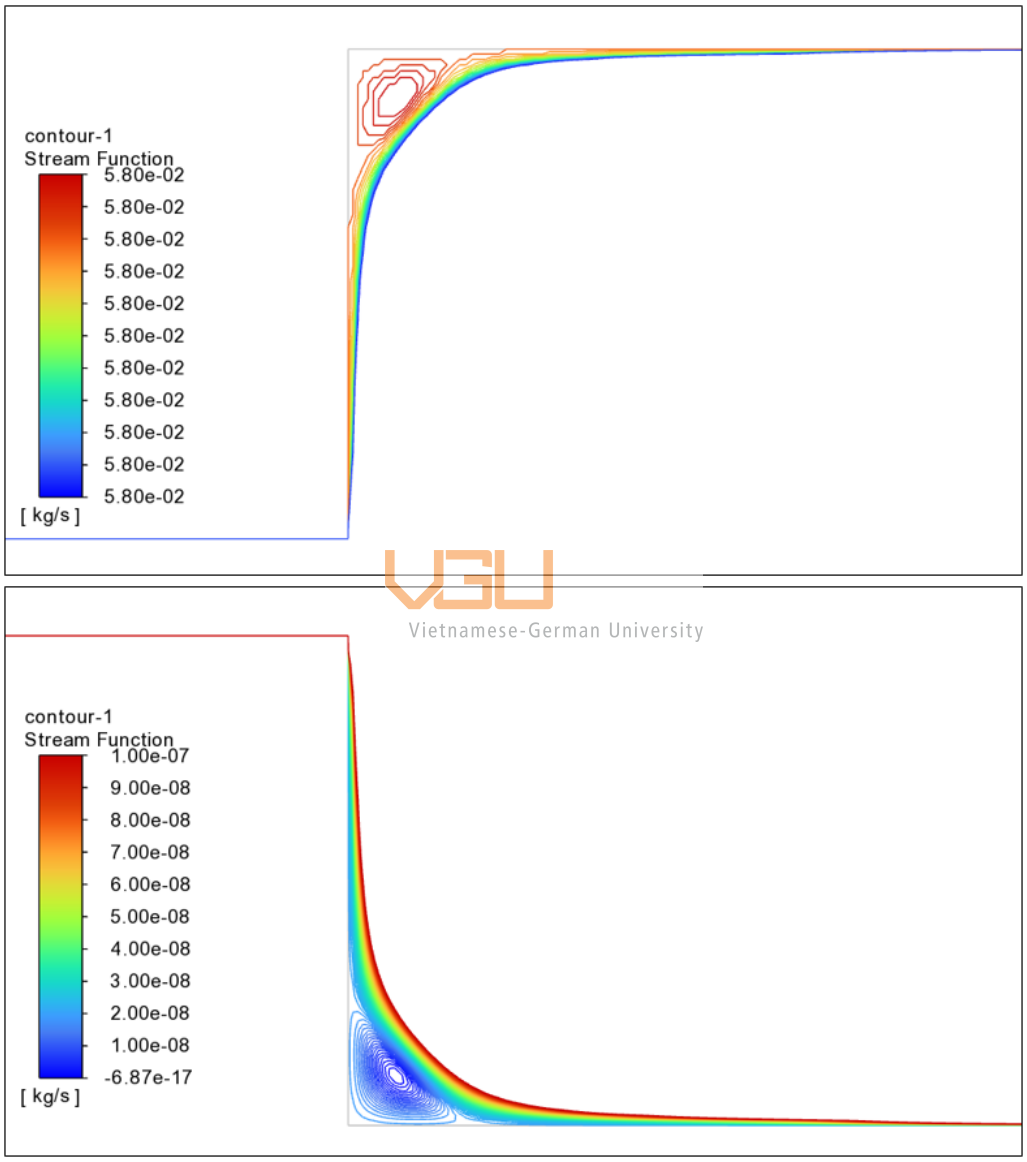

FIGURE 4.8: Recirculation of Kao 28.5wt% $Re = 40$

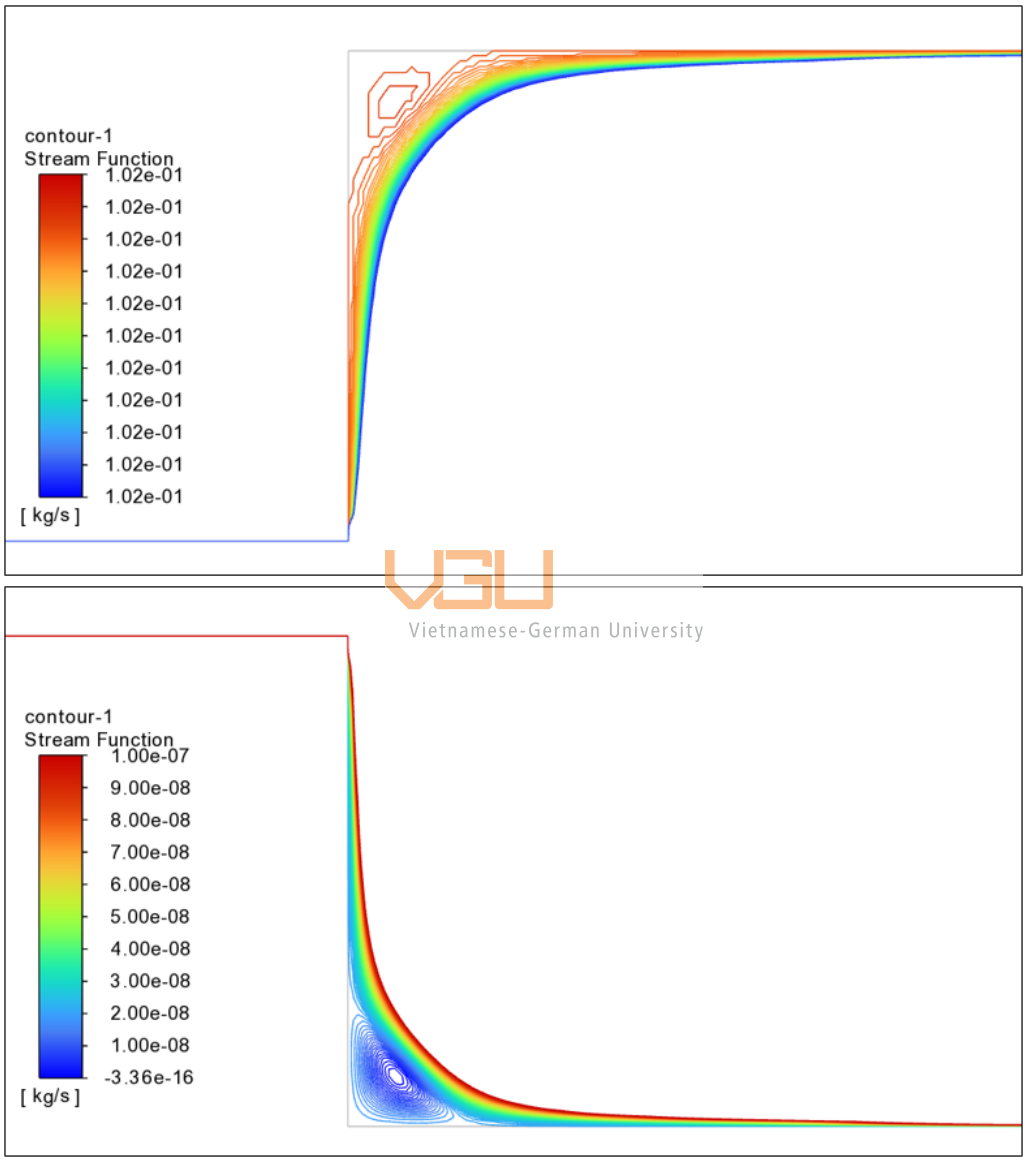

FIGURE 4.9: Recirculation of Kao 28.5wt% $Re = 70$

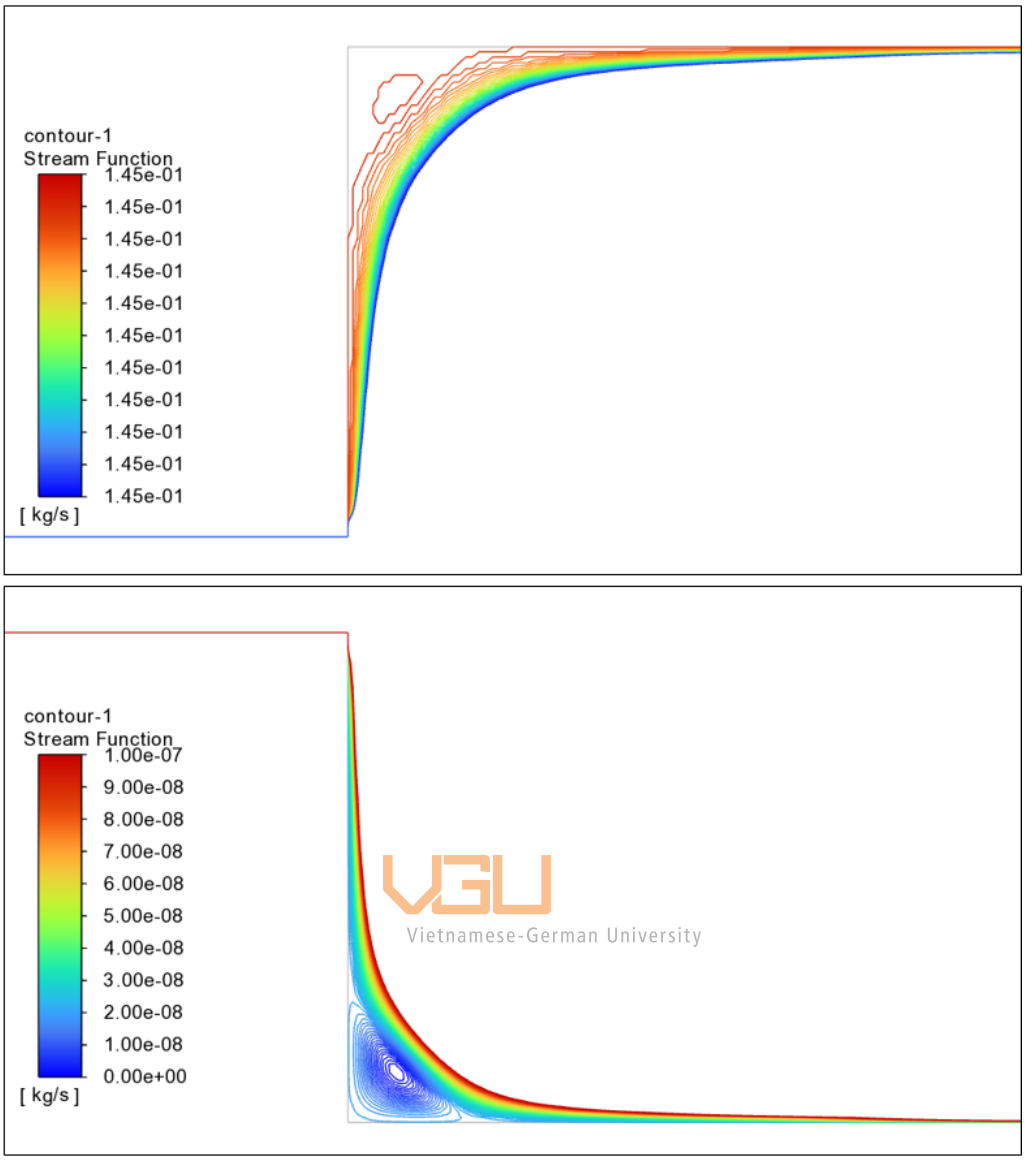

FIGURE 4.10: Recirculation of Kao 28.5wt% $Re = 100$

With the power-law index $n = 1$, the Reynolds number range in this study ($20 \leq Re \leq 100$) does not surpass the critical Reynolds number for the bifurcation to make the recirculations be asymmetric. The shape of those swirls are almost the same; since the limitation of the software, it cannot be displayed the identical curves onto the images. And they just have a significant small difference in their size (up to 1×10^{-7}), it will be more detailed in the section 4.1.3.

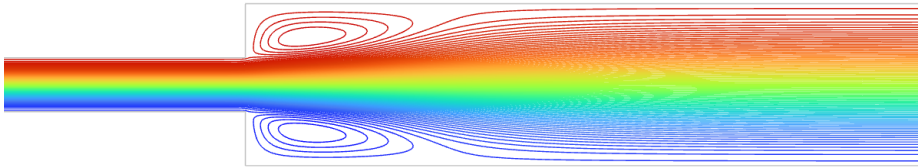

FIGURE 4.11: Water streamline at Re = 40

When comparing them with a traditional Newtonian fluid, for instance, water in this case. There are bigger swirls at both corners. Also, these streamlines are perfect symmetric through the x-axis for low value of *Re*.

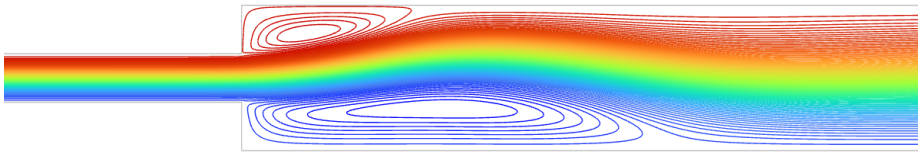

FIGURE 4.12: Water streamline at Re = 70

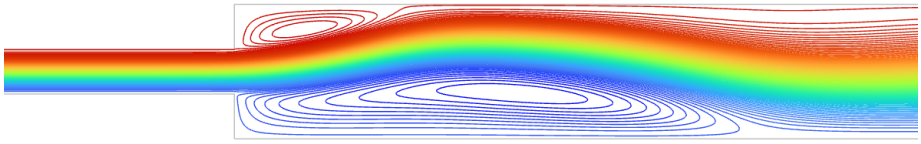

FIGURE 4.13: Water streamline at Re = 100

But when the *Re* is become bigger, the streamline creates asymmetric swirls at two corners. The upper swirl is smaller comparing to the one at the bottom. Since the viscosity of water is lower than the Kao-family, its streamline is more visible within the software's limitation. The result here is also agreed with the work of Dhinakaran [16] for larger value of Reynolds number. Since the viscosity of water is low, the phenomenon happens earlier with just a little increase in Reynolds number.

4.1.2 X-wall shear stress

To have a better view at the characteristic length X_a and X_b of the recirculations, it is crucial to analyze a graph illustrating the x-wall shear stress to observe alterations in pressure. As the pressure switches in the direction along the x-axis, the recirculation segment stops and at that point the boundary between this segment and the bifurcation flow is defined. Notably, due to the symmetric nature of both recirculations, the outcomes for the top wall need not be presented separately, as they mirror those for the bottom wall.

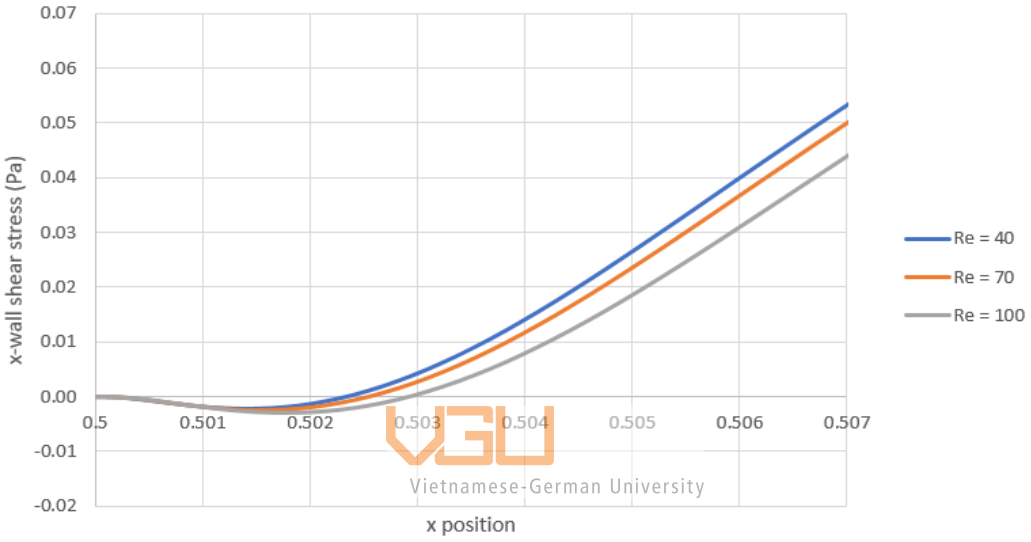

FIGURE 4.14: X-wall shear stress at bottom wall for Kao15

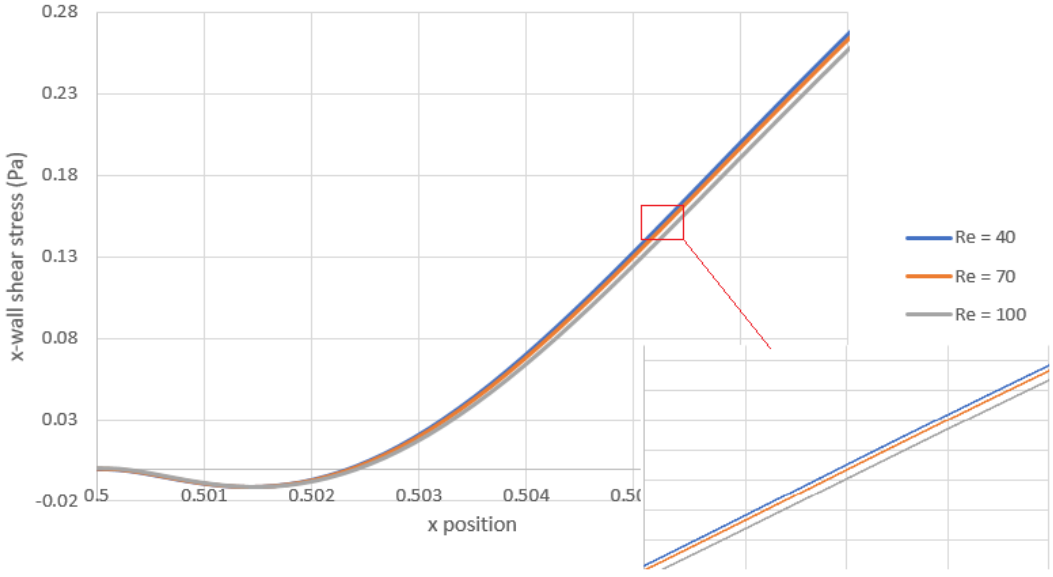

FIGURE 4.15: X-wall shear stress at bottom wall for Kao20

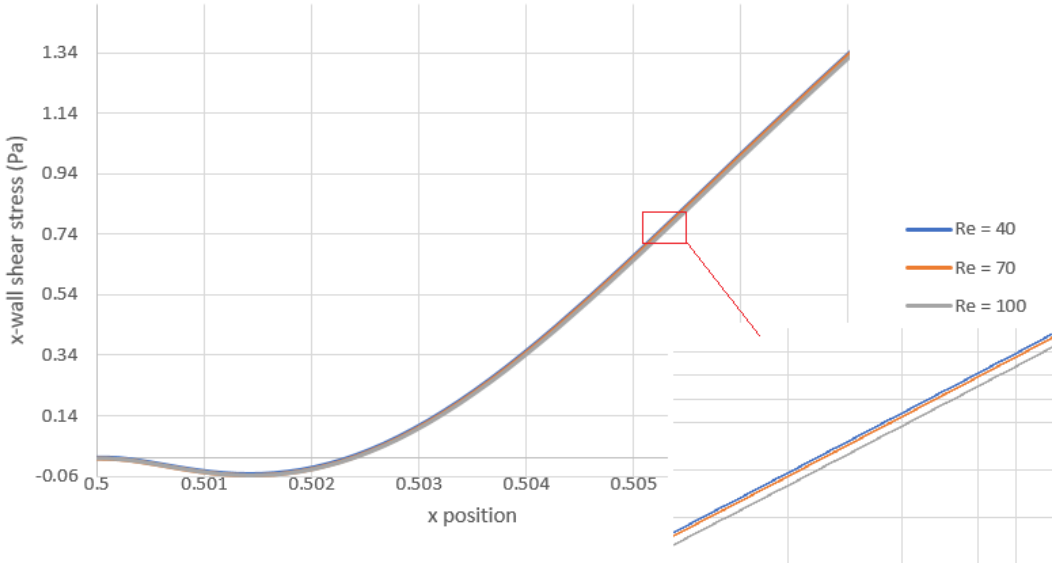

FIGURE 4.16: X-wall shear stress at bottom wall for Kao28.5

In Fig. 4.14 the distinctions in the length X_a are evident, as three lines are distinctly separated when crossing the x-axis. However, in the Fig. 4.15 and Fig. 4.16, the trends of the lines converge. This phenomenon can be attributed to an increase in critical shear stress, leading to heightened fluid inertia and consequently requiring a greater force to drag the group. Due to the relatively modest Reynolds numbers, the difference is insufficient to yield a huge leap in the characteristic length X_a.

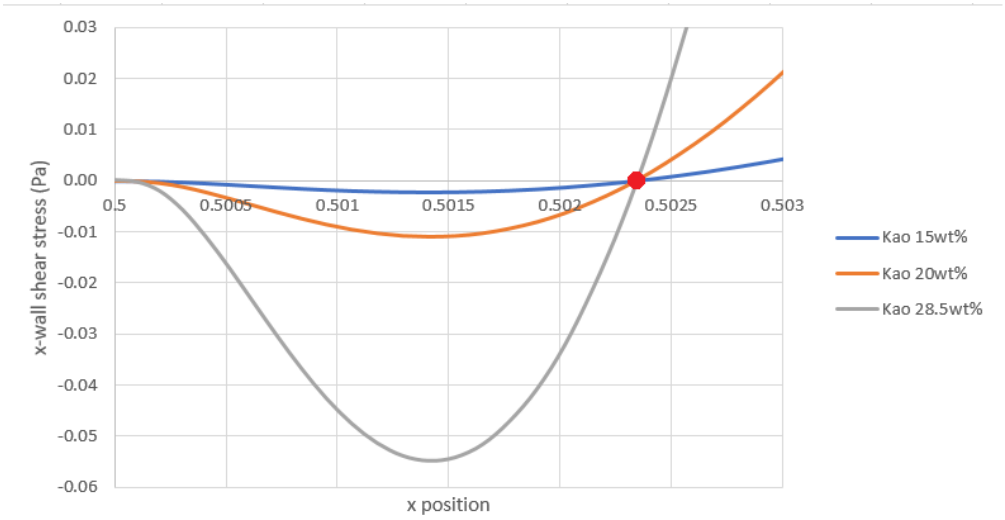

FIGURE 4.17: X-wall shear stress at bottom wall for $Re = 40$ with different fluids

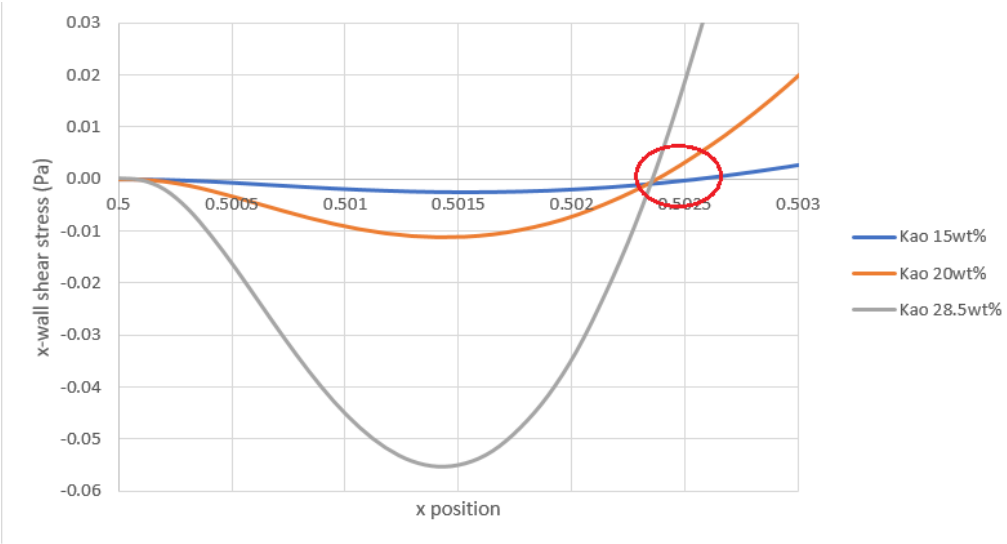

FIGURE 4.18: X-wall shear stress at bottom wall for $Re = 70$ with different fluids

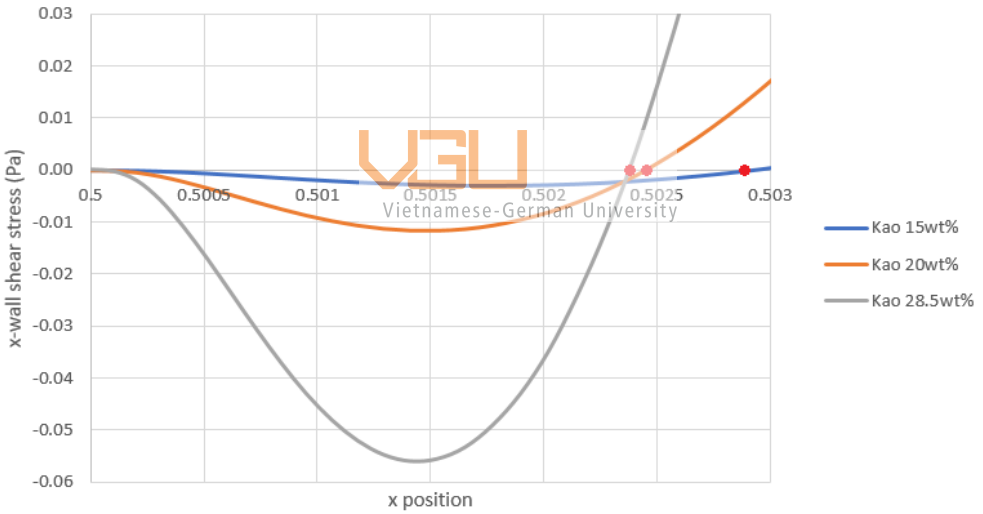

FIGURE 4.19: X-wall shear stress at bottom wall for $Re = 100$ with different fluids

When the Reynolds number is small (Fig. 4.17), the characteristic length appears to exhibit reduced dependence on fluid properties, with closely aligned values for X_a among different fluids. However, as the Reynolds number increases, the points of directional change in the X-wall shear stress diverge more significantly. In the instance of the highest Reynolds number considered, $Re = 100$ (Fig. 4.19), noteworthy disparities emerge in the placement of points of interest. This discrepancy can be attributed to the substantial inertia present in the Kao 28.5wt% fluid, which delay the amplification of recirculation to a greater extent.

4.1.3 The characteristic length

To generalize the characteristic length changing across the Reynolds number for three different fluids, the Fig. 4.20 shows the graph for X_a respect to Reynolds numbers.

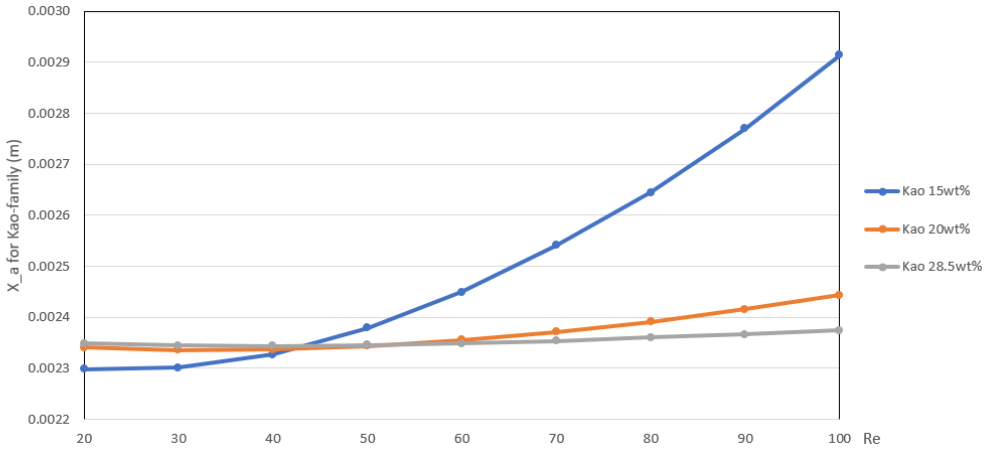

FIGURE 4.20: The characteristic length X_a respects to Reynolds number

The X_a for either Kao 15wt% and Kao 20wt% starts lower than that for Kao 28.5wt%, which respect to the Reynolds number from 20 to 40. In contrast, when the Reynolds gets bigger, for around 43, the trend for X_a is moving in the opposite way. Kao 15wt% and Kao 20wt% both witness a steadily raise in the X_a and the Kao 15wt% has a steeper slope. Meanwhile, the Kao 28.5wt% still grows up but with a much more lower slope and falls behind those two after around $Re = 43$.

As in Table 4.1, the difference for X_a and X_b is insignificant, so it does not exhibit a notable impact on the overall trends. Consequently, the decision is made to keep the graph for X_b out of the visual representation to maintain clarity and focus on the more influential aspects of the data.

Re	X_a Kao15	X_b Kao15	X_a Kao20	X_b Kao20	X_a Kao28.5	X_b Kao28.5
40	0.0023278	0.0023276	0.0023371	0.0023366	0.0023447	0.0023441
70	0.0025412	0.0025411	0.0023711	0.0023709	0.0023544	0.0023541
100	0.0029149	0.0029149	0.0024434	0.0024433	0.0023750	0.0023748

TABLE 4.1: Difference between X_a and X_b for Kaolinite-s

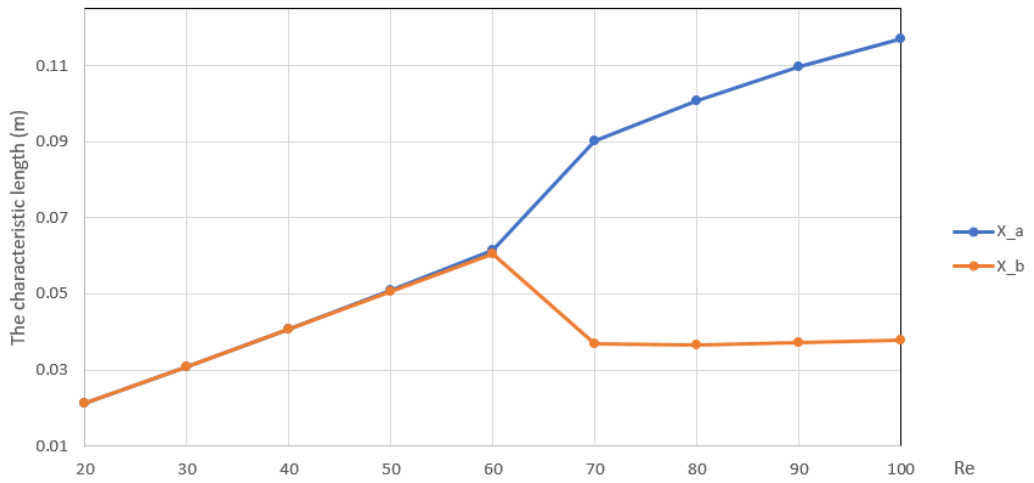

FIGURE 4.21: The characteristic length X_a and X_b for Water

The asymmetric flow phenomenon happens earlier for water, occurring approximately within the range of $60 < Re \leq 70$. The bifurcation during sudden expansion creates two distinct swirls at the bottom and top salient corners. Notably, a significant transition is observed in the characteristic length X_a, leading to a marked shift in flow behavior towards turbulence at $Re = 70$. This turbulent flow pattern is demonstrated in the streamline representation shown in Section 4.1.1.

4.2 Velocity profile

The part below shows all images about velocity vector profile for conducted cases:

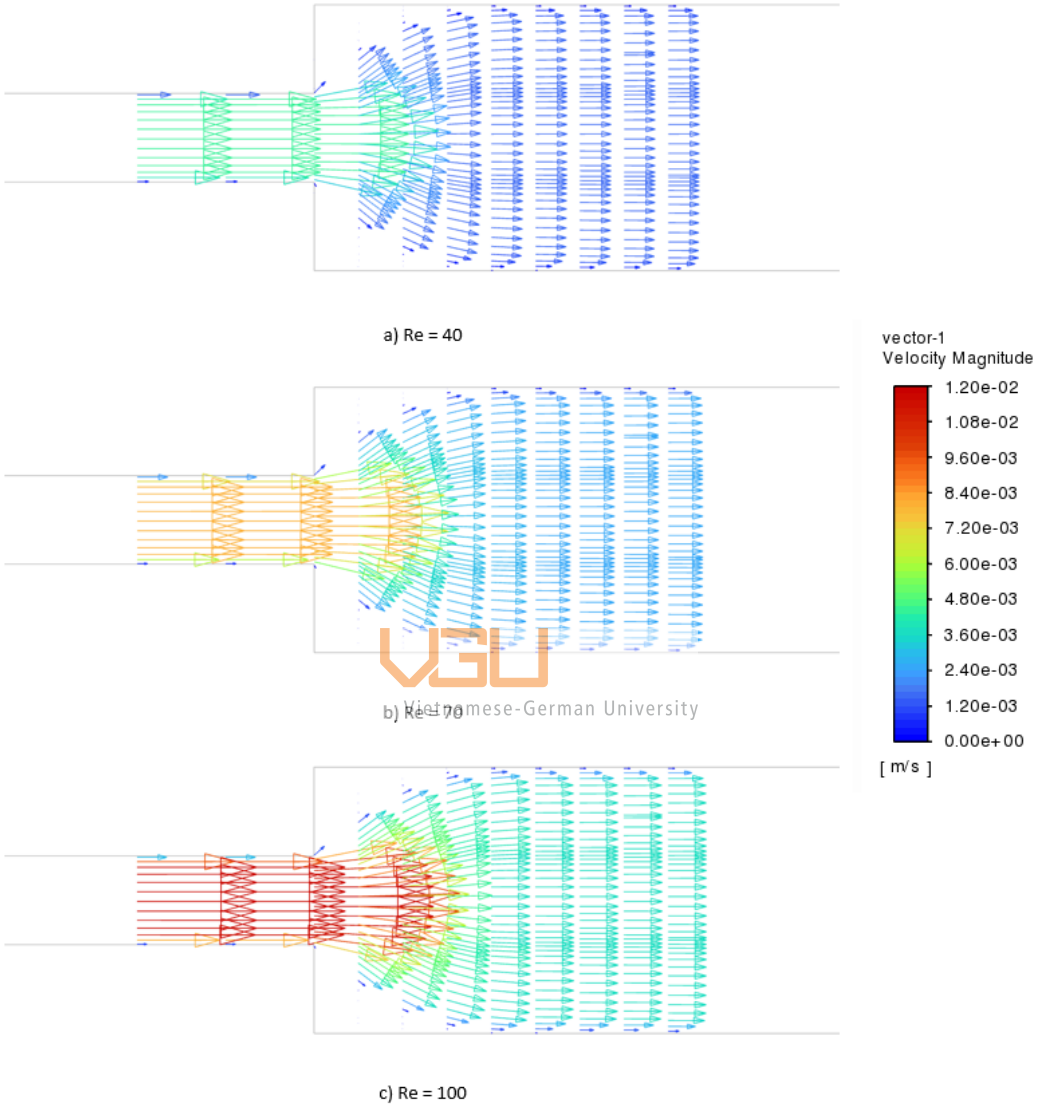

FIGURE 4.22: The velocity profile for Kao 15wt% a) Re = 40; b) Re = 70; c) Re = 100

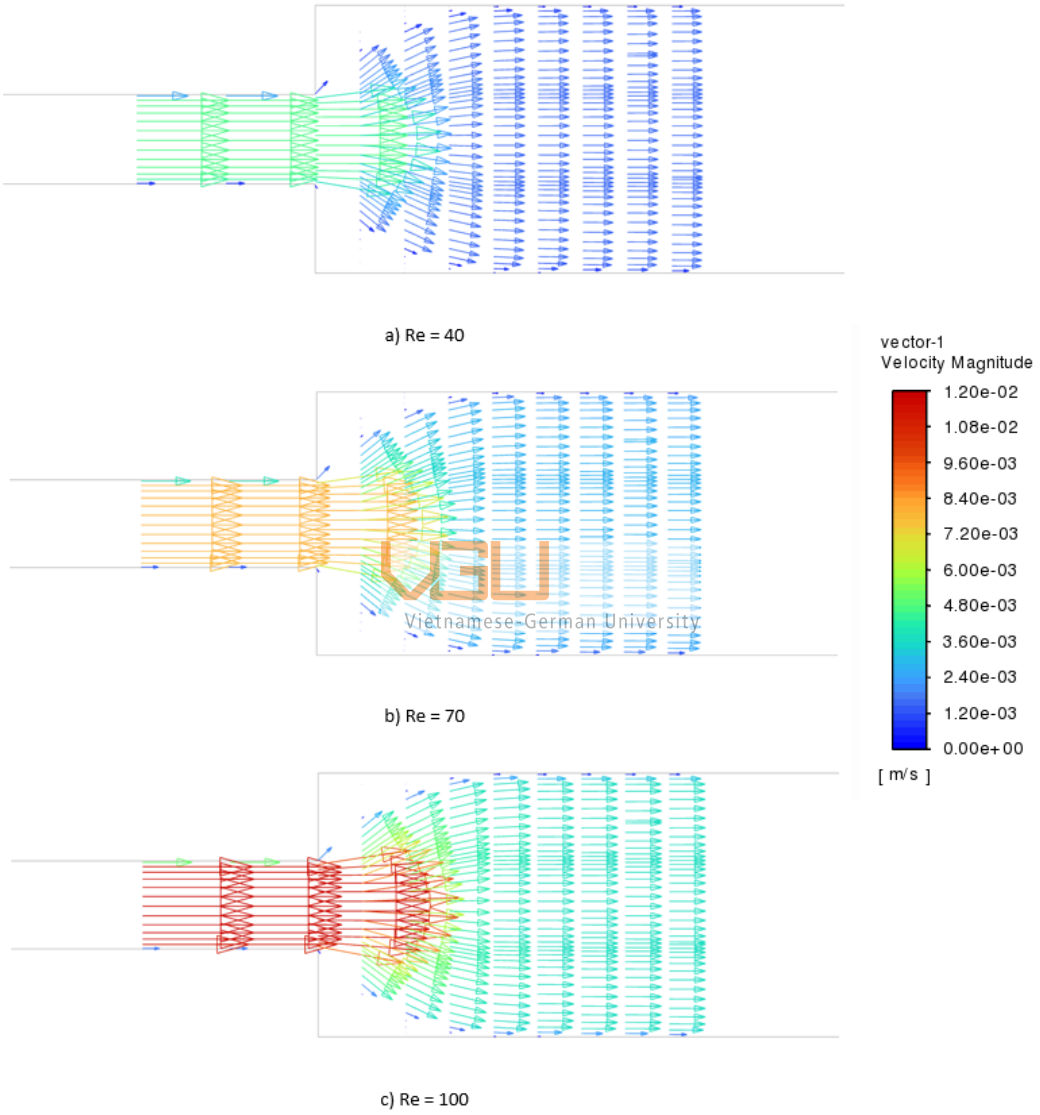

FIGURE 4.23: The velocity profile for Kao 20wt% a) Re = 40; b) Re = 70; c) Re = 100

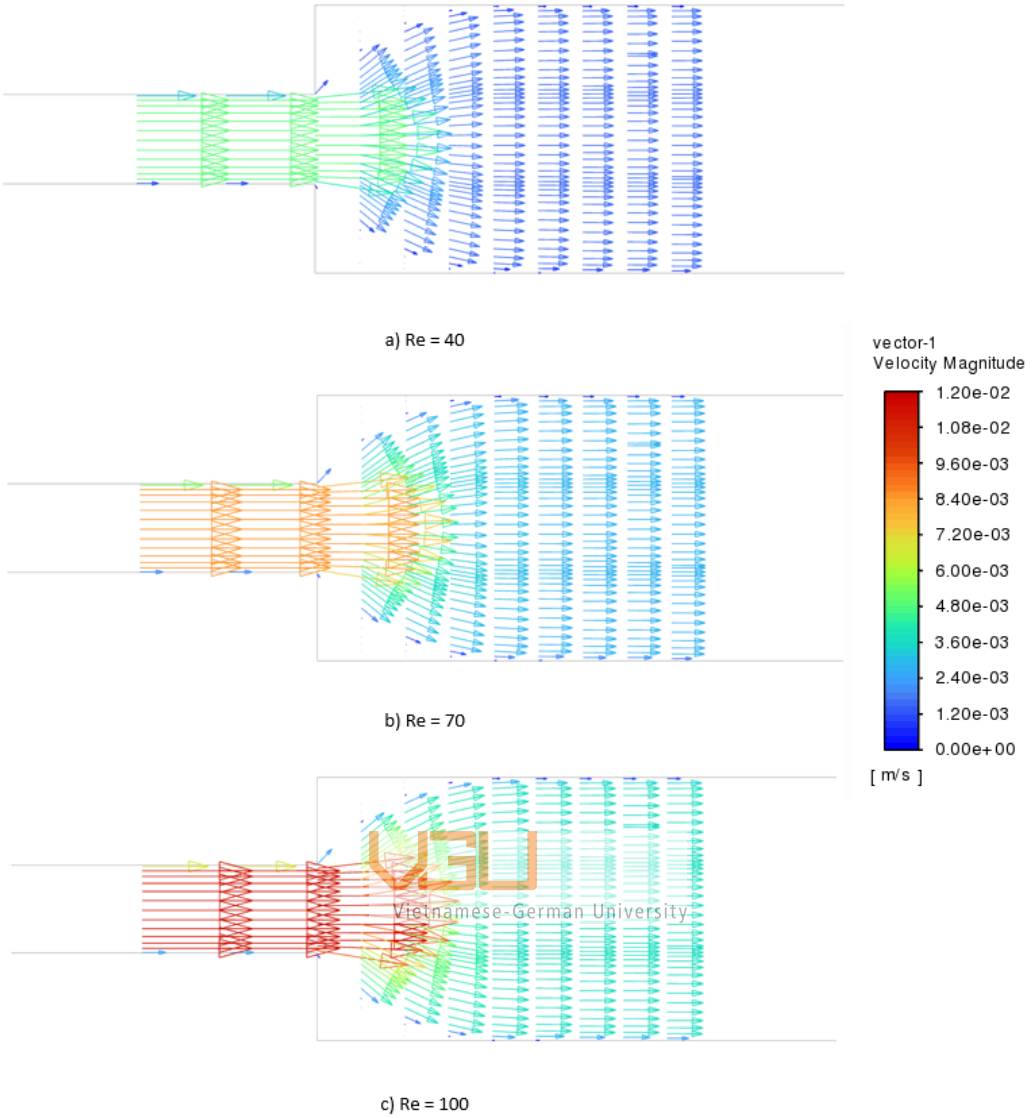

FIGURE 4.24: The velocity profile for Kao 28.5wt% a) Re = 40; b) Re = 70; c) Re = 100

The inlet velocity increases with the rising Reynolds number. At the bottleneck position, bifurcation commences, leading to a decrease in flow speed as it diffuses into the expansion chamber. The diminished velocity is approximately one-third of the original velocity from the upstream channel, as denoted by the color gradient. This finding aligns with theoretical predictions derived from the conservation of flow rate.

$$\dot{V}_{upstream} = \dot{V}_{downstream} => u_{us}A_{us} = u_{ds}A_{ds} => u_{us} = 3u_{ds}$$

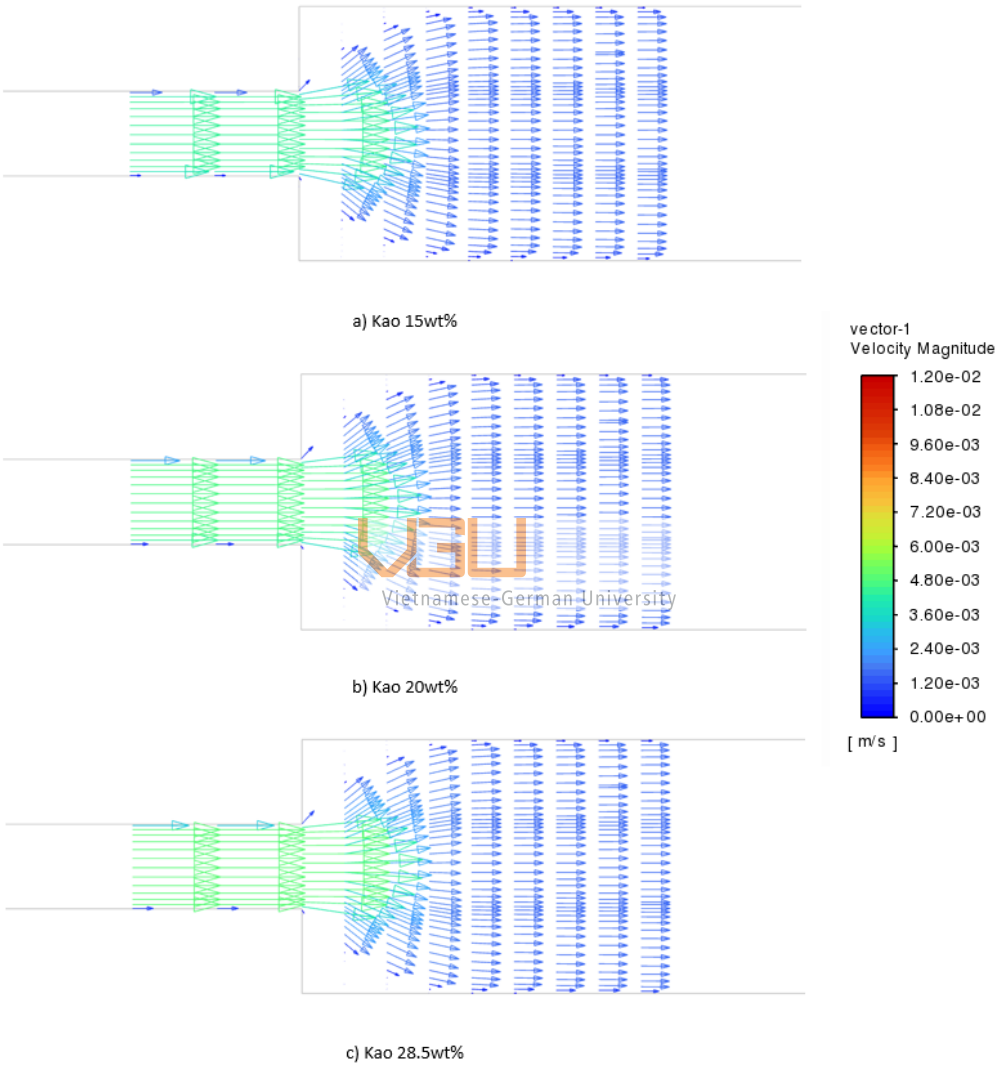

FIGURE 4.25: The velocity profile for Re = 40 a) Kao 15wt%; b) Kao 20wt%; c) Kao 28.5wt%

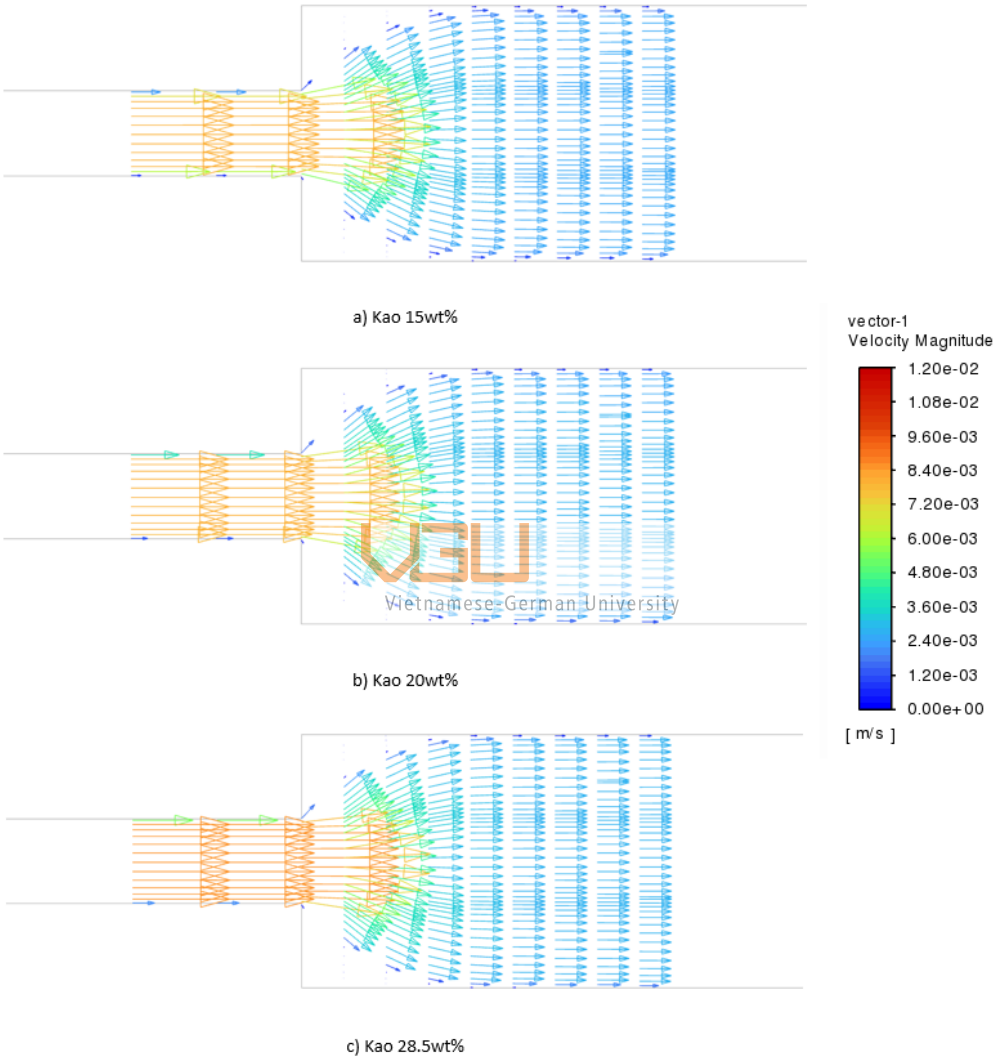

FIGURE 4.26: The velocity profile for Re = 70 a) Kao 15wt%; b) Kao 20wt%; c) Kao 28.5wt%

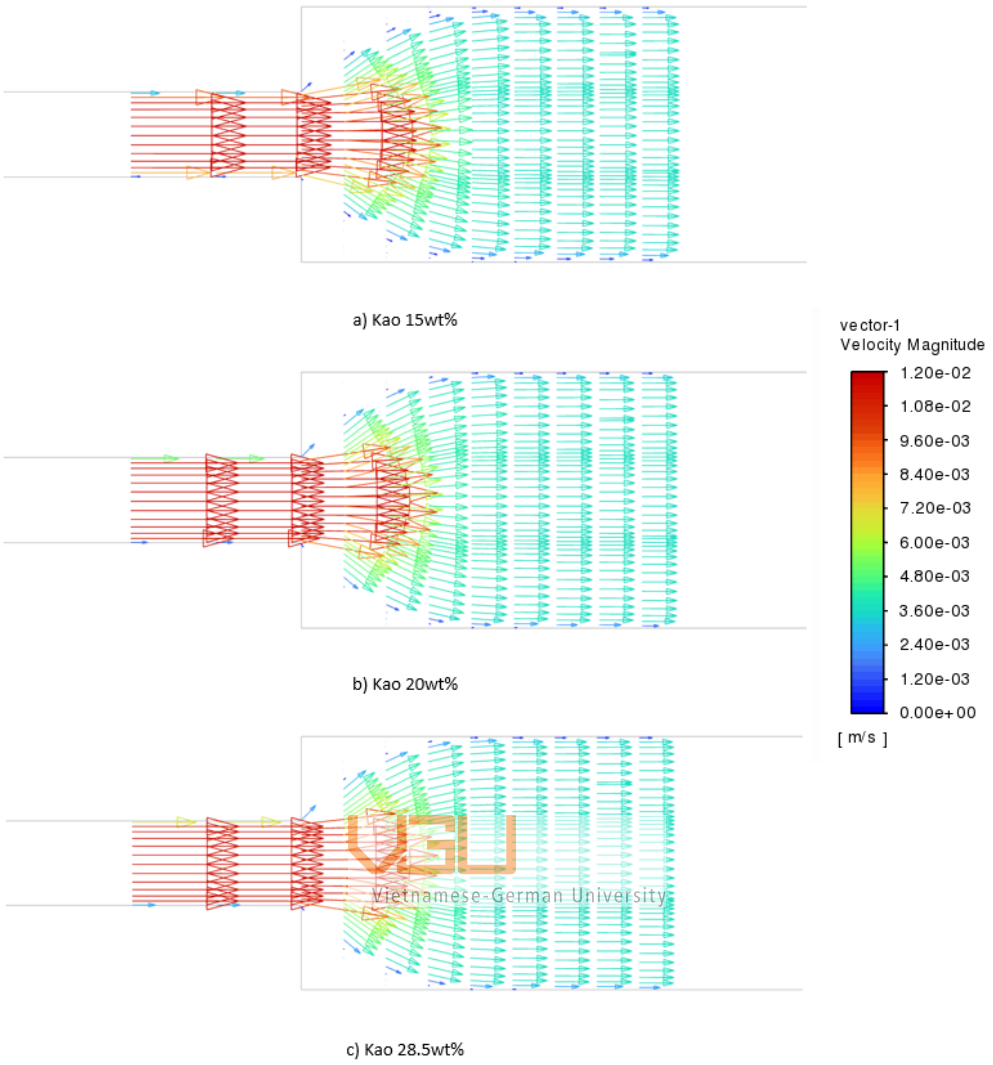

FIGURE 4.27: The velocity profile for Re = 100 a) Kao 15wt%; b) Kao 20wt%; c) Kao 28.5wt%

When combining three Kaolinite fluids at the same Reynolds number, the differences in the results are relatively minor. The most notable variation occurs at the bottleneck, specifically during the sudden expansion, where the velocity vector of the Kaolinite fluid with higher density shows a larger magnitude. However, at low Reynolds numbers (refer to Fig. 4.25), this discrepancy is not substantial.

4.3 Darcy friction factor

Utilizing Equation 2.5, the Darcy friction factors were computed based on simulation results. Simultaneously, the theoretical Darcy factors were determined using Equation 2.6.

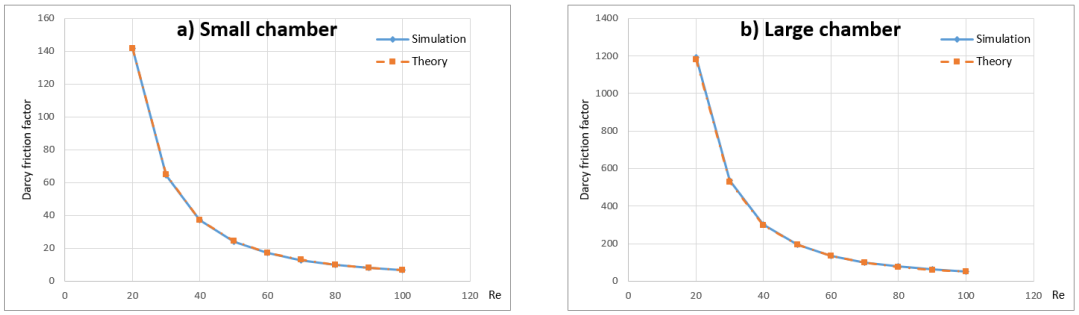

FIGURE 4.28: Comparing theoretical and simulated Darcy friction factors for Kao 15wt% a)Small chamber b) Large chamber

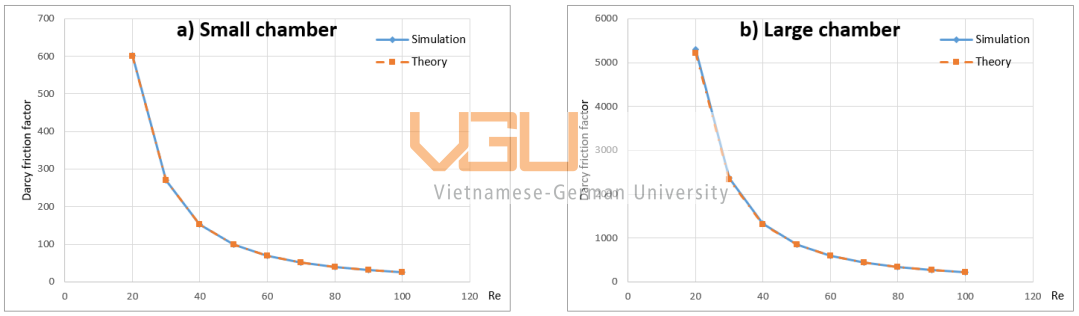

FIGURE 4.29: Comparing theoretical and simulated Darcy friction factors for Kao 20wt% a)Small chamber b) Large chamber

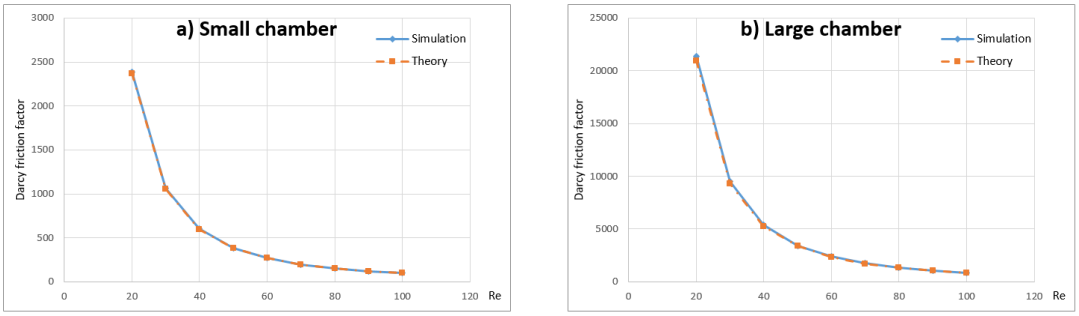

FIGURE 4.30: Comparing theoretical and simulated Darcy friction factors for Kao 28.5wt% a)Small chamber b) Large chamber

The calculation process proceeds as follows: the simulation results are easily obtained through direct calculation from the Darcy-Weisbach equation (Equation 2.5). On the other hand, the theoretical results pose a challenge as the equation demands an iterative approach. Overcoming this intricacy necessitated the implementation of a Python programming solution to iteratively derive the theoretical values.

The outcomes exhibit remarkable similarity between the theoretical and simulation results, with an error margin of less than or equal to 2.07%. The reduction in velocity post the sudden expansion event results in a larger Darcy factor in the larger chamber compared to the smaller one, despite employing the same investigatory fluid. Across various working fluids, a substantial increase in the Darcy factor is observed when the rheological properties of the fluid manifest increased resistance to flow.

Chapter 5

Conclusion

This thesis investigates a study case for three different types of Kaolinite fluid family, for which Kao 15wt%, 20wt% and 28.5wt%. The expansion ratio (EH), which is the height of output channel divided by the height of the input channel is 3. The mesh was used with 124450 cells. The numerical approach was conducted for the low Reynolds number ranging from 20 to 100.
The main conclusion for this study is listed as the following:

- After the sudden expansion, the Kao-fluids exhibit symmetric recirculations at salient corners, aligning with findings from previous studies on power-law index $n = 1$ fluids at low Reynolds number. For water the flow becomes asymmetrical starting from Re = 60 or so; however, for Kao 15wt%, 20wt%, 28.5wt%, the flow is still symmetrical at Re = 100.

- The characteristic length exhibits minimal dependence on the properties of fluids when the Reynolds number is small. Instead, it is more likely to be influenced by the Reynolds number itself, particularly when dealing with low-velocity flows.

- The characteristic length undergoes a change in its trend at a critical Reynolds number across the Kao-family fluids. It is significantly smaller for non-Newtonian fluids compared to Newtonian fluids.

- The velocity profiles for different Kao-fluids tend to be nearly identical at the same Reynolds number. The most significant deviation occurs precisely at the re-entrant corner.

- Post-expansion, the larger chamber shows a higher Darcy factor than the smaller one, despite using the same fluid. Across fluids, a notable Darcy factor increase is observed with increased rheological resistance to flow.

List of Figures

List of Tables

List of Symbols

τ	Shear Stress	$\mathrm{N\,m^{-2}}$
τ_0	Yield Strength	$\mathrm{N\,m^{-2}}$
μ	Viscosity	$\mathrm{N\,s\,m^{-2}}$ or $\mathrm{Pa\,s}$
$\dot{\gamma}$	Shear Rate	$\mathrm{s^{-1}}$
η	Apparent Viscosity	$\mathrm{N\,s\,m^{-2}}$ or $\mathrm{Pa\,s}$
ρ	Density	$\mathrm{kg\,m^{-3}}$
h	Small Channel Width	m
H	Large Channel Width	m
L_C	Small Channel Length	m
L_E	Large Channel Length	m
X_a	Primary Vortex Characteristic Length	m
X_b	Secondary Vortex Characteristic Length	m
u	Velocity	$\mathrm{m\,s^{-1}}$
n	Power-law Index	Dimensionless
f	Darcy Friction Factor	Dimensionless
f_L	Laminar Flow Darcy Friction Factor	Dimensionless
$\overline{v}$	Mean Velocity	$\mathrm{m\,s^{-1}}$
Re	Reynolds Number	Dimensionless
He	Hedstrom Number	Dimensionless
D_h	Hydraulic Diameter of the Pipe	m

List of Abbreviations

ErF	**E**lectro**r**heological **F**luid
MrF	**M**agneto**r**heological **F**luid
ER	**E**xpansion **R**atio
CFD	**C**omputational **F**luid **D**ynamics
FVM	**F**inite **V**olume **M**ethod
PDEs	**P**artial **D**ifferential **E**quation**s**
SIMPLE	**S**emi-**I**mplicit **M**ethod for **P**ressure-**L**inked **E**quations

Bibliography

[1] *What is viscosity ? states newton's law of viscosity define newtonian and non-newtonian fluid*, 2015. [Online]. Available: https://mechaengineerings.wordpress.com/2015/05/25/viscosity/.

[2] *Non-newtonian fluid*. [Online]. Available: https://en.wikipedia.org/wiki/Non-Newtonian_fluid.

[3] R. Chhabra and J. Richardson, "Chapter 1 - non-newtonian fluid behaviour," in *Non-Newtonian Flow and Applied Rheology (Second Edition)*, R. Chhabra and J. Richardson, Eds., Second Edition, Oxford: Butterworth-Heinemann, 2008, pp. 1–55, ISBN: 978-0-7506-8532-0. DOI: https://doi.org/10.1016/B978-0-7506-8532-0.00001-9. [Online]. Available: https://www.sciencedirect.com/science/article/pii/B9780750685320000019.

[4] A. Behera, "Smart fluid," in *Advanced Materials: An Introduction to Modern Materials Science*. Cham: Springer International Publishing, 2022, pp. 193–223, ISBN: 978-3-030-80359-9. DOI: 10.1007/978-3-030-80359-9_6. [Online]. Available: https://doi.org/10.1007/978-3-030-80359-9_6.

[5] *Viscosity of blood*, 2022. [Online]. Available: https://cvphysiology.com/hemodynamics/h011.

[6] *Ketchup is not just a condiment: It is also a non-newtonian fluid*, 2021. [Online]. Available: https://www.scientificamerican.com/article/ketchup-is-not-just-a-condiment-it-is-also-a-non-newtonian-fluid/.

[7] F. Durst, A. Melling, and J. H. Whitelaw, "Low reynolds number flow over a plane symmetric sudden expansion," *Journal of Fluid Mechanics*, vol. 64, no. 1, 111–128, 1974. DOI: 10.1017/S0022112074002035.

[8] W. Cherdron, F. Durst, and J. H. Whitelaw, "Asymmetric flows and instabilities in symmetric ducts with sudden expansions," *Journal of Fluid Mechanics*, vol. 84, no. 1, 13–31, 1978. DOI: 10.1017/S0022112078000026.

[9] R. M. Fearn, T. Mullin, and K. A. Cliffe, "Nonlinear flow phenomena in a symmetric sudden expansion," *Journal of Fluid Mechanics*, vol. 211, 595–608, 1990. DOI: 10.1017/S0022112090001707.

[10] D. Drikakis, "Bifurcation phenomena in incompressible sudden expansion flows," *Physics of Fluids*, vol. 9, no. 1, pp. 76–87, Jan. 1997, ISSN: 1070-6631. DOI: 10.1063/1.869174. eprint: https://pubs.aip.org/aip/pof/article-pdf/9/1/76/12270991/76_1_online.pdf. [Online]. Available: https://doi.org/10.1063/1.869174.

[11] S. Mishra and K. Jayaraman, "Asymmetric flows in planar symmetric channels with large expansion ratio," *International Journal for Numerical Methods in Fluids*, vol. 38, no. 10, pp. 945–962, Apr. 2002. DOI: 10.1002/fld.242.

[12] R Manica and A. De Bortoli, "Simulation of sudden expansion flows for power-law fluids," *Journal of Non-Newtonian Fluid Mechanics*, vol. 121, no. 1, pp. 35–40, 2004, ISSN: 0377-0257. DOI: https://doi.org/10.1016/j.jnnfm.2004.03.009. [Online]. Available: https://www.sciencedirect.com/science/article/pii/S0377025704000667.

[13] P. Neofytou, "Transition to asymmetry of generalised newtonian fluid flows through a symmetric sudden expansion," *Journal of Non-Newtonian Fluid Mechanics*, vol. 133, no. 2, pp. 132–140, 2006, ISSN: 0377-0257. DOI: https://doi.org/10.1016/j.jnnfm.2005.12.004. [Online]. Available: https://www.sciencedirect.com/science/article/pii/S0377025705002715.

[14] R. Poole and B. Ridley, "Development-length requirements for fully developed laminar pipe flow of inelastic non-newtonian liquids," *Journal of Fluids Engineering-transactions of The Asme - J FLUID ENG*, vol. 129, Oct. 2007. DOI: 10.1115/1.2776969.

[15] P. Ternik, "Planar sudden symmetric expansion flows and bifurcation phenomena of purely viscous shear-thinning fluids," *Journal of Non-Newtonian Fluid Mechanics*, vol. 157, no. 1, pp. 15–25, 2009, ISSN: 0377-0257. DOI: https://doi.org/10.1016/j.jnnfm.2008.09.002. [Online]. Available: https://www.sciencedirect.com/science/article/pii/S0377025708001699.

[16] S. Dhinakaran, M. Oliveira, F. Pinho, and M. Alves, "Steady flow of power-law fluids in a 1:3 planar sudden expansion," *Journal of Non-Newtonian Fluid Mechanics*, vol. 198, pp. 48–58, 2013, ISSN: 0377-0257.

DOI: https://doi.org/10.1016/j.jnnfm.2013.01.006. [Online]. Available: https://www.sciencedirect.com/science/article/pii/S0377025713000323.

[17] *Darcy–weisbach equation*. [Online]. Available: https://en.wikipedia.org/wiki/Darcy%E2%80%93Weisbach_equation.

[18] *Bingham plastic*. [Online]. Available: https://en.wikipedia.org/wiki/Bingham_plastic.

Appendix A

Supplementary data

TABLE A.1: Properties for Kao 15wt%

Density ($kg\,m^{-3}$)	Viscosity ($kg\,m^{-1}\,s^{-1}$)	Yield stress, τ_0 (Pa)	Power-law index	Critical shear rate (s^{-1})	Reynolds number	Inlet velocity ($m\,s^{-1}$)
1101.694915	0.001182007	0.08	1	0.01	20	0.002146
1101.694915	0.001182007	0.08	1	0.01	30	0.003219
1101.694915	0.001182007	0.08	1	0.01	40	0.004292
1101.694915	0.001182007	0.08	1	0.01	50	0.005364
1101.694915	0.001182007	0.08	1	0.01	60	0.006437
1101.694915	0.001182007	0.08	1	0.01	70	0.007510
1101.694915	0.001182007	0.08	1	0.01	80	0.008583
1101.694915	0.001182007	0.08	1	0.01	90	0.009656
1101.694915	0.001182007	0.08	1	0.01	100	0.010729

TABLE A.2: Properties for Kao 20wt%

Density ($kg\,m^{-3}$)	Viscosity ($kg\,m^{-1}\,s^{-1}$)	Yield stress, τ_0 (Pa)	Power-law index	Critical shear rate (s^{-1})	Reynolds number	Inlet velocity ($m\,s^{-1}$)
1140.350877	0.00126564	0.4	1	0.01	20	0.002220
1140.350877	0.00126564	0.4	1	0.01	30	0.003330
1140.350877	0.00126564	0.4	1	0.01	40	0.004439
1140.350877	0.00126564	0.4	1	0.01	50	0.005549
1140.350877	0.00126564	0.4	1	0.01	60	0.006659
1140.350877	0.00126564	0.4	1	0.01	70	0.007769
1140.350877	0.00126564	0.4	1	0.01	80	0.008879
1140.350877	0.00126564	0.4	1	0.01	90	0.009989
1140.350877	0.00126564	0.4	1	0.01	100	0.011099

TABLE A.3: Properties for Kao 28.5wt%

Density ($kg\,m^{-3}$)	Viscosity ($kg\,m^{-1}\,s^{-1}$)	Yield stress, τ_0 (Pa)	Power-law index	Critical shear rate (s^{-1})	Reynolds number	Inlet velocity ($m\,s^{-1}$)
1212.686567	0.001450325	2	1	0.01	20	0.002392
1212.686567	0.001450325	2	1	0.01	30	0.003588
1212.686567	0.001450325	2	1	0.01	40	0.004784
1212.686567	0.001450325	2	1	0.01	50	0.005980
1212.686567	0.001450325	2	1	0.01	60	0.007176
1212.686567	0.001450325	2	1	0.01	70	0.008372
1212.686567	0.001450325	2	1	0.01	80	0.009568
1212.686567	0.001450325	2	1	0.01	90	0.010764
1212.686567	0.001450325	2	1	0.01	100	0.011960

TABLE A.4: Properties for Water

Density ($kg\,m^{-3}$)	Viscosity ($kg\,m^{-1}\,s^{-1}$)	Reynolds number	Inlet velocity ($m\,s^{-1}$)
997.0474	0.00089	20	0.001785
997.0474	0.00089	30	0.002678
997.0474	0.00089	40	0.003571
997.0474	0.00089	50	0.004463
997.0474	0.00089	60	0.005356
997.0474	0.00089	70	0.006248
997.0474	0.00089	80	0.007141
997.0474	0.00089	90	0.008034
997.0474	0.00089	100	0.008926

TABLE A.5: Values of X_a for Kao 15, Kao 20, and Kao 28.5

Re	X_a for Kao 15	X_a for Kao 20	X_a for Kao 28.5
20	0.002298	0.002341	0.002349
30	0.002301	0.002336	0.002345
40	0.002327	0.002337	0.002344
50	0.002379	0.002344	0.002346
60	0.002449	0.002355	0.002349
70	0.002541	0.002371	0.002354
80	0.002645	0.002391	0.002360
90	0.002770	0.002416	0.002366
100	0.002914	0.002443	0.002374

TABLE A.6: X_a and X_b values for Water

Re	X_a for Water	X_b for Water
20	0.021194	0.021188
30	0.030850	0.030819
40	0.040840	0.040722
50	0.050971	0.050666
60	0.061350	0.060515
70	0.090249	0.036788
80	0.100878	0.036659
90	0.109681	0.037180
100	0.117082	0.037926

TABLE A.7: X_a and X_b values for Kao 15, Kao 20, and Kao 28.5

Re	X_a Kao 15	X_b Kao 15	X_a Kao 20	X_b Kao 20	X_a Kao 28.5	X_b Kao 28.5
40	0.0023278	0.0023276	0.0023371	0.0023366	0.0023447	0.0023441
70	0.0025412	0.0025411	0.0023711	0.0023709	0.0023544	0.0023541
100	0.0029149	0.0029149	0.0024434	0.0024433	0.0023750	0.0023748

A.1 Python Code

Below is the Python code used for calculations:

```
rho = #Insert Density
v = [
    #Insert list of velocity
]
diameter = #Insert hydraulic diameter
mu = #Insert Viscosity
tau = #Insert Yield Strength

for velocity in v:
    #Calculating Reynolds number
    Re = rho * velocity * diameter / mu

    #Calculating Hedstrom number
    He = rho * (diameter**2) * tau / (mu**2)

    #Init. Darcy friction factor
    f_L0 = 64 / Re

    #Init. residual
    residual = 1

    #Iteration process
    while residual >= 0.0001:
        f_L = 64 / Re * (1 + He / (6 * Re) - 64 / 3 * ((He**4) / ((f_L0
            **3) * (Re**7))))
        residual = abs(f_L - f_L0)
        f_L0 = f_L

    #Print result
    print(f_L)
```